Delft University of Technology

Document Version
Final published version

Licence
CC BY-NC-ND

Citation (APA)
Buccino, F., Matteucci, L., Mirzaali, M., Zadpoor, A., & Vergani, L. M. (2026). Architected metamaterials for enhanced ductility and strength through bio-inspired twinning strategies and topology optimization. *Materials and Design*, *268*, Article 116576. https://doi.org/10.1016/j.matdes.2026.116576

Important note
To cite this publication, please use the final published version (if applicable).
Please check the document version above.

Copyright
In case the licence states "Dutch Copyright Act (Article 25fa)", this publication was made available Green Open Access via the TU Delft Institutional Repository pursuant to Dutch Copyright Act (Article 25fa, the Taverne amendment). This provision does not affect copyright ownership.
Unless copyright is transferred by contract or statute, it remains with the copyright holder.

Sharing and reuse
Other than for strictly personal use, it is not permitted to download, forward or distribute the text or part of it, without the consent of the author(s) and/or copyright holder(s), unless the work is under an open content license such as Creative Commons.

Takedown policy
Please contact us and provide details if you believe this document breaches copyrights.
We will remove access to the work immediately and investigate your claim.

This work is downloaded from Delft University of Technology.

Materials & Design 268 (2026) 116576

Contents lists available at ScienceDirect

Materials & Design

journal homepage: www.elsevier.com/locate/matdes

Architected metamaterials for enhanced ductility and strength through bio-inspired twinning strategies and topology optimization

F. Buccino [a,b], L. Matteucci [a], M. Mirzaali [c], A. Zadpoor [c], L.M. Vergani [a,b,*]

[a] Department of Mechanical Engineering (DMEC), Politecnico di Milano, Via La Masa 1, 20156 Milan, Italy
[b] IRCCS Galeazzi-Sant'Ambrogio, Via Cristina Belgioioso 173, 20157 Milan, Italy
[c] Department of Biomechanical Engineering, Faculty of Mechanical Engineering, Delft University of Technology (TU Delft), Mekelweg 2, 2628 CD Delft, the Netherlands

ARTICLE INFO

Keywords:
Architected metamaterials
Twinning
Topology optimization
3D printing
Bio-inspired strategy

ABSTRACT

Architected materials offer promisingly high strength-to-weight and stiffness-to-weight ratios but are traditionally limited in ductility. This work proposes a bio-inspired design framework that combines twinning-inspired deformation control with topology optimization to overcome the conventional strength–ductility trade-off in architected metamaterials. Unlike previous approaches that improve either ductility or strength individually, the proposed methodology integrates stress-delocalizing twin boundaries (TBs) with connectivity-enhancing topology optimization to simultaneously improve both properties. Three configurations (*baseline*, *twinned*, and *optimized*) are fabricated with appproximately identical mass and tested under uniaxial compression. Full-field strain mapping is obtained via digital image correlation, and finite-element analysis is used to simulate stress distribution and failure mechanisms. Results show that TBs significantly increase ductility by ≈15–20 %, while the *optimized* lattice achieves a > 97 % increase in deformation capacity and ≈118 % increase in peak load relative to the base structure, in agreement with the numerical simulations. The *optimized* unit cell exhibits a bending-dominated response, facilitating larger plastic deformations and extended shear-band formation, in contrast to the stretching-dominated behavior of base and twinned cells. These promising findings will provide a foundation for damage-programmable metamaterials in applications requiring controlled deformation and high structural resilience.

1. Introduction

Architected metamaterials represent an emergent class of engineered structures in which geometry and topology, rather than intrinsic material composition, govern macroscopic properties [1–4]. Unlike stochastic cellular solids, lattice-based architectures offer systematic tunability of stiffness, strength, and anisotropy, enabling multifunctional performance ranging from wave guiding and acoustic damping to controlled energy absorption and fluid transport [5–14]. The maturation of additive manufacturing technologies has allowed these geometrically programmed materials to be fabricated across nano-, micro-, and macro-scales, consolidating their role in applications that demand lightweight performance with high structural efficiency, such as aerospace, automotive, and biomedicine [15–20].

The mechanical performance of lattice metamaterials is dictated by their dominant deformation modes. Stretching-dominated topologies generally achieve the highest stiffness- and strength-to-weight ratios but tend to fail catastrophically through brittle strut fracture or localized buckling [21–25]. Conversely, bending-dominated lattices promote distributed deformation and higher energy dissipation, but at the expense of peak load-bearing capacity [26–28]. In both cases, structural collapse is controlled by the formation of strain-localization patterns that resemble shear bands, which are mesoscale analogues of crystallographic slip planes in conventional solids [29–31]. This analogy underscores the fundamental strength–ductility trade-off observed in metamaterials: architectures optimized for strength exhibit limited ductility and sudden failure, whereas those designed for energy absorption dissipate load more gradually but sacrifice ultimate strength [32–37].

Overcoming this trade-off remains one of the central challenges in the design of next-generation architected materials.

A promising route to circumvent this limitation can be identified by drawing inspiration from deformation mechanisms in both crystalline solids and natural biological materials (Fig. 1a). In metals, when

* Corresponding author at: Department of Mechanical Engineering (DMEC), Politecnico di Milano, Via La Masa 1, 20156 Milan, Italy.
E-mail address: laura.vergani@polimi.it (L.M. Vergani).

https://doi.org/10.1016/j.matdes.2026.116576
Received 12 March 2026; Received in revised form 21 June 2026; Accepted 8 July 2026
Available online 15 July 2026
0264-1275/© 2026 The Author(s). Published by Elsevier Ltd. This is an open access article under the CC BY-NC-ND license (http://creativecommons.org/licenses/by-nc-nd/4.0/).

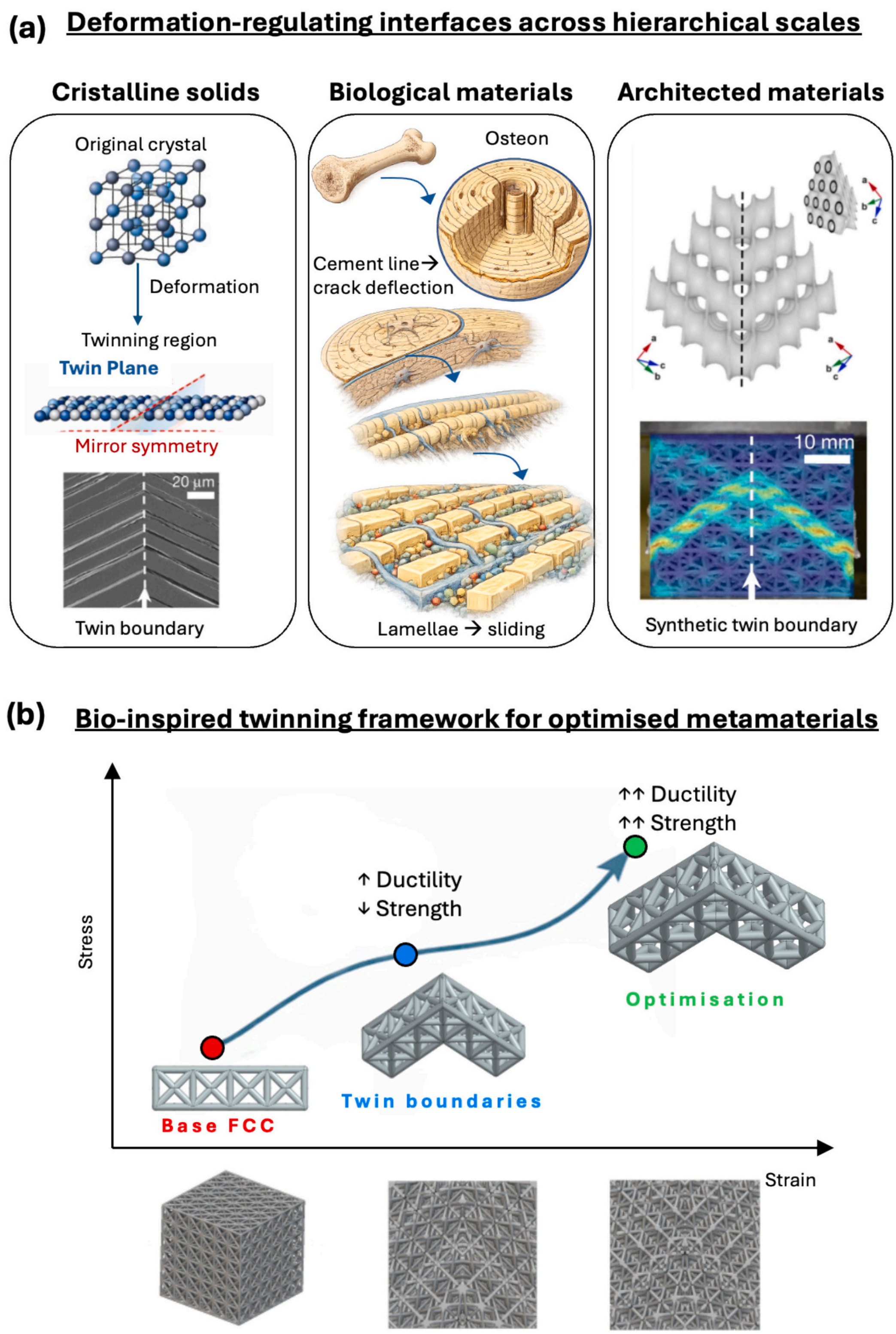

Fig.1. Bio-inspired deformation-regulating interfaces: from crystallographic twinning to hierarchical bone and architected materials. (a) Deformation twinning in metals is shown through atomic schematics and microscopy images, highlighting twin planes and coherent twin boundaries with mirror symmetry. This concept is extended to bone, where hierarchical interfaces, from the femur and osteons to lamellae and nanoscale collagen–mineral assemblies, control strain distribution, crack deflection, and energy dissipation. Synthetic lattice structures with engineered twin-like boundaries demonstrate analogous deformation mechanisms at the mesoscale. (b) Schematic performance map of this research showing how introducing twin boundaries into architected lattices enables tunable mechanical behavior, evolving from a base Face Centered Cubic (FCC) structure to optimized architectures that achieve simultaneous increases in strength and ductility. In the bottom part an overview of the metamaterials is shown.

dislocation slip alone cannot accommodate plastic strain, deformation twinning emerges as an alternative mode of plasticity [7,15–17,28,38–41]. Twin boundaries not only provide new planes for dislocation glide but also act as barriers to slip transmission, redistributing stress, increasing strain hardening, and delaying strain localization [17]. This dual functionality enables alloys such as Mg, Ti, brass, and certain steels to simultaneously achieve strength and ductility, a combination typically considered mutually exclusive [16,28]. An analogous principle is widespread in natural structural materials, where interfaces and hierarchical design act to arrest, deflect, and redistribute stresses. In bone, microcracks are guided and deflected along lamellar boundaries, enhancing energy dissipation and delaying catastrophic failure [42–44]. Nacre achieves remarkable toughness by forcing crack deviation and progressive energy absorption through its brick-and-mortar architecture [45,46]. Both biological and crystalline systems thus exploit planes of symmetry or interfaces that act as regulators of strain localization, and this convergence suggests a general bio-inspired principle of deformation twinning: stress-redistributing planes, whether in crystals, biominerals, or engineered structures, impart ductility and toughness by disrupting shear localization and promoting distributed deformation [47–55].

Translating this paradigm to architected metamaterials, recent studies have demonstrated that the deliberate introduction of twinning-inspired interfaces within lattice geometries can serve as mesoscale analogues of crystallographic twin boundaries [28,38,56]. These engineered interfaces regulate strain localization by interrupting shear-band propagation, redistributing stresses across multiple load-transfer pathways, and promoting more progressive failure mechanisms. For example, Wu et al. (2022) proposed architected twin mechanical metamaterials capable of suppressing local shear-band formation and delaying catastrophic collapse [3], while Song et al. (2022) demonstrated that crystal-twinning-inspired lattices can simultaneously enhance stiffness, strength, and toughness through the incorporation of twin boundaries [3,57]. More broadly, crystal-inspired interfaces such as *meta*-grain boundaries have also been shown to redirect strain localization and improve damage tolerance in architected materials [26]. These approaches introduce a form of "synthetic plasticity" into metamaterials, enabling progressive deformation and energy dissipation without modifying the base constituent material.

In parallel, topology optimization has emerged as a powerful computational strategy for tailoring the mechanical response of architected materials through the redistribution of material [58] and the modification of load-transfer pathways [54,59]. Optimized lattices frequently exhibit enhanced stiffness, strength, and structural stability [60,61] as a result of reduced stress concentrations and improved connectivity [62–65]. However, these benefits are often accompanied by increased strain localization and more abrupt failure, thereby limiting ductility and damage tolerance [66,67].

Despite the significant progress achieved by both approaches, they have largely evolved independently. Twinning-inspired architectures primarily focus on controlling deformation localization and enhancing damage tolerance, whereas topology optimization is generally employed to maximize strength and structural efficiency. Consequently, the potential interaction between stress-delocalization mechanisms induced by twin boundaries and connectivity enhancement induced by topology optimization remains largely unexplored [50,68,69]. Furthermore, each strategy independently addresses only one side of the strength-ductility dilemma: twinning improves deformation capacity but may reduce peak load-bearing capability, while topology optimization enhances strength but often promotes localized failure. This unresolved trade-off motivates the development of integrated design strategies capable of simultaneously improving both strength and ductility.

The present study addresses this challenge by proposing a bio-inspired synergistic framework that integrates twinning-inspired design principles with topology optimization.

The underlying hypothesis is that twinning and topology optimization contribute through distinct but complementary mechanisms. Twinning planes primarily act as deformation-regulating interfaces that redistribute stresses, delay strain localization, and promote controlled failure pathways, thereby enhancing ductility. In contrast, topology optimization primarily improves load-bearing efficiency by stabilizing load paths and reducing stress concentrations. The combination of these two mechanisms is therefore expected to overcome the mechanical antagonism that has thus far constrained lattice metamaterials, enabling simultaneous improvements in damage tolerance, deformation capacity, and strength. Importantly, the objective of the present study is not to demonstrate that twinning alone maximizes mechanical performance. Rather, twinning is employed as a bio-inspired architectural strategy to modify the deformation mode of the lattice and introduce alternative stress redistribution pathways. Topology optimization is subsequently applied to exploit these pathways and improve structural efficiency. The proposed design framework therefore treats twinning as the mechanism governing deformation localization and topology optimization as the mechanism governing load transfer, allowing their individual and combined contributions to be systematically investigated.

To prove this hypothesis, three classes of architected lattices are systematically investigated: a *baseline* geometry, a *twinning*-inspired variant, and a topology-*optimized* design. By comparing their deformation modes, stress redistribution patterns, and failure mechanisms, the study seeks to disentangle the respective contributions of twinning and optimization, and to determine whether their integration enables simultaneous enhancement of strength and ductility (Fig. 1b).

The novelty of this work resides in its translation of deformation twinning, a mechanism historically confined to metallurgy and broadly mirrored in biological systems, into the design logic of architected metamaterials, where it functions as a synthetic analogue of plasticity. By coupling this bio-inspired mechanism with the computational strategy of topology optimization, this study introduces a pathway to architected lattices that are both strong and ductile, thereby providing a conceptual and methodological advance in the design of damage-tolerant metamaterials.

2. Materials and methods

The methodological framework integrates architected design, computational modeling, topology optimization, additive manufacturing, and experimental validation to demonstrate that the deliberate incorporation of synthetic TBs and optimization strategies at the mesoscale enables stress redistribution, suppression of shear band localization, activation of multiple deformation pathways, and enhanced energy dissipation in architected metamaterials, thereby transposing the twinning-induced plasticity paradigm from crystalline solids to lattice architectures.

2.1. Architected metamaterials design and optimization process

The design process is structured around the comparative analysis of three lattice topologies:

(i) Baseline FCC lattice

The baseline lattice is a conventional FCC architecture, selected as a canonical structure for architected metamaterials due to its relatively isotropic mechanical response, straightforward fabrication, and extensive documentation in the literature [16,17]. The FCC configuration, while mechanically robust under moderate load, is prone to instability once local strut buckling initiates, resulting in highly localized deformation and rapid strength degradation. This makes it an ideal control case to benchmark the proposed strengthening mechanisms.

The lattice is modeled in nTopology 4.0.5, using a line-segment representation of struts aligned with the cubic axes. The unit cell size (lattice parameter) is set at 6.66 mm, and the strut diameter at 0.95 mm, balancing structural resolution against manufacturability with vat photopolymerization-based 3D printing. The infill domain is defined as a cube of 40 × 40 × 40 mm, corresponding to ~ 6 unit cells per side, which is sufficient to reproduce bulk-like behavior in both simulations and experiments [7]. The FCC lattice is oriented without any rotation relative to the bounding cube, ensuring full periodicity and alignment between the infill and the bounding geometry.

This baseline design provides the mechanical ground state against which twinning- and optimization-induced effects can be assessed.

It is worth mentioning that the FCC topology has been deliberately selected as the reference architecture because of its relatively isotropic mechanical response and well-established deformation behavior. This choice minimizes the influence of orientation-dependent effects and enables the specific contribution of the twin boundary to stress redistribution, deformation localization, and failure propagation to be more clearly identified.

(ii) Twinned FCC lattice

The second design introduces twinning as a mesoscale strengthening mechanism. Twinning is here realized by designing two distinct *meta*-grains, each containing FCC unit cells oriented at 45° relative to the bounding box along two axes. The two halves are separated by a central plane of symmetry, across which the unit cells are mirrored, generating an artificial TB. This plane effectively acts as a mesoscale analogue of crystallographic twin boundaries: it divides the structure into regions of mirrored orientation while retaining lattice continuity across the interface.

The unit cell modeling followed a two-step transformation:

a) rotation: the FCC unit cell was rotated by 45° around the x- and y-axes within a 20 × 40 × 40 mm sub-volume, creating a "grain" of reoriented lattice. The 45° rotation was selected as a crystallographic-inspired design choice: this orientation enables the construction of two mirror-symmetric *meta*-grains separated by a central twin boundary, analogous to twinned or polycrystal-inspired architected materials in which misoriented domains redirect shear-band propagation and stabilize deformation. Mechanically, the 45° orientation reduces the dominance of struts aligned with the compression axis and introduces inclined load paths, promoting stress redistribution and shear-band development instead of the layer-wise collapse observed in the baseline FCC lattice;

b) mirroring: this rotated sub-volume was mirrored across the yz-plane to produce a 40 × 40 × 40 mm full lattice containing a central TB.

The motivation for this design is grounded in both materials science and biomechanics. In crystalline metals, TBs are known to block dislocation transmission while simultaneously providing alternative glide planes, thus enhancing both strength and ductility [7,39]. In biological composites such as bone and nacre, analogous interfaces act as crack deflectors and stress redistributors, extending toughness [70,71]. By embedding an analogous TB in an architected lattice, it is aimed to generate synthetic plasticity, where stress is redistributed across the boundary and failure is delayed by controlled crack deflection or stress bifurcation.

One important challenge in constructing mirrored lattices is the presence of edge discontinuities at the domain boundaries, where struts may not perfectly align due to the reorientation of unit cells. To avoid premature edge-driven fracture, a 0.5 mm-thick external shell is added around the structure. This shell acts as a mechanical stabilizer, suppressing artefacts during compression testing and ensuring that failure initiates within the bulk of the lattice, not at its periphery.

The *twinned* FCC lattice thus represents an intermediate case, isolating the contribution of twinning boundaries to ductility enhancement while still retaining the original, non-optimized strut topology.

(iii) Optimized twinned FCC lattice

The third structure integrates topology optimization with twinning to design an architected material that combines the ductility-enhancing role of TBs with stress-minimization in the unit cell geometry.

Optimization is carried out in Altair Inspire 2023.1, employing a Sequential Quadratic Programming (SQP) algorithm. The optimization domain is restricted to the FCC unit cell, which was subjected to periodic boundary conditions and simulated under compressive loading.

The topology optimization problem can be expressed as: $\min_{\rho(x)} \sigma_{VM,max}$, where $\sigma_{VM,max}$ is the maximum von Mises stress within the design domain, and $\rho(x)$ represents the local material density distribution. The objective is therefore to reduce stress concentrations while preserving the target material content and geometric symmetry of the unit cell.

Constraints include: a) preservation of lattice periodicity and FCC symmetry; b) minimum strut diameter of 1 mm to ensure printability; c) target material removal fraction of 80%, consistent with lightweight design practices. It should be noted that the 80% material removal constraint refers exclusively to the topology optimization process performed on the initial solid design space. This parameter does not represent a reduction in the mass of the final lattice architecture relative to the baseline design. Rather, it defines the amount of material available to the optimizer during topology generation and was selected to produce a unit cell with a relative density comparable to that of the reference FCC architecture.

Von Mises stress was selected as the optimization metric because it is directly associated with the onset of yielding through the distortional energy criterion. Since the objective of the present work is to delay stress localization and failure initiation within the lattice, minimizing von Mises stress provides a physically meaningful approach for promoting more homogeneous load transfer and reducing local stress concentrations. Alternative optimization formulations based on p-norm aggregation could potentially generate different topological solutions and provide additional insight into the relationship between optimization objectives and deformation mechanisms.

Unlike the conventional straight struts of the baseline FCC, the optimized struts preserved the nominal printable diameter of 1 mm but exhibited curvilinear, stress-guided trajectories generated through topology optimization, features that have been shown to improve buckling resistance and energy absorption [72,73]. The *optimized* unit cell is reconstructed into a lattice by replicating the new topology and introducing a central TB using the same mirroring strategy as the previous design. As with the twinned FCC lattice, an external shell is added to the *optimized* structure to eliminate edge-related discontinuities and to ensure reproducibility of mechanical testing. The optimization process redistributed material within the unit cell while preserving periodicity, manufacturability, and equivalent relative density. In particular, the initially straight FCC members evolved into smooth curved load paths, reducing abrupt directional changes in force transmission and promoting a more homogeneous stress distribution throughout the structure. Compared with the baseline FCC unit cell, the optimized architecture also exhibited an approximately 75% increase in nodal connectivity, with the number of shared nodal intersections per unit-cell face increasing from one central connection to four distributed nodal connections. These geometric modifications promoted multiple load-transfer pathways and contributed to the transition from a predominantly stretching-dominated response toward a bending-dominated deformation regime.

For clarity, an overview of the geometrical characteristics of the considered architectures is reported in Table 1.

2.2. Analytical framework for mass-invariant design

To isolate the effect of architectural modifications from density-driven strengthening effects, all lattice configurations were designed

Table 1
Geometrical characteristics of the investigated architectures.

Parameter	Baseline FCC	Twinned FCC	Optimized FCC
Unit-cell size	6.66 mm	6.66 mm	6.66 mm
Strut diameter	0.95 mm	1.00 mm	1.00 mm
Relative density	0.2034	0.2034	0.2034
Specimen dimensions	40 × 40 × 40 mm^3	40 × 40 × 40 mm^3	40 × 40 × 40 mm^3
Twin boundary	No	Yes	Yes
Unit-cell orientation	0°	45°	45°

under constant-mass conditions. Relative density (ρ) was adopted as the primary geometric descriptor and defined as Eq.1:

$$\rho = \frac{V_t}{V} \tag{1}$$

where V_t is the solid volume of the cellular material and V is the total volume of the unit cell.

For the baseline FCC unit cell, the relative density was calculated as:

$$\rho = \frac{\frac{12}{4}\bullet L \bullet A + \frac{12}{2}\bullet L \bullet A\sqrt{2}}{L^3} \tag{2}$$

where L is the unit-cell size and A is the cross-sectional area of the struts.

For the optimized unit cell, the relative density was evaluated as:

$$\rho = \frac{\frac{L}{2\sqrt{2}}\bullet \frac{8}{2}\bullet 6 \bullet A + L \bullet \frac{12}{4}\bullet A}{L^3} \tag{3}$$

To quantify the topological modification introduced by optimization, a connectivity increase was defined as:

$$\Delta C = \frac{C_{opt} - C_{base}}{C_{base}} \times 100 \tag{4}$$

where C_{base} and C_{opt} are the connectivity indices of the baseline and optimized unit cells, respectively.

The effect of topology optimization on structural stability was evaluated through simplified beam-model analyses. The critical-load increase was calculated as:

$$\Delta P_{cr} = \frac{P_{cr,opt} - P_{cr,base}}{P_{cr,base}} \times 100 \tag{5}$$

where $P_{cr,base}$ and $P_{cr,opt}$ are the critical loads obtained from linear perturbation buckling analyses of the baseline and optimized unit cells.

2.3. Numerical modeling

The finite element models are developed in Abaqus CAE 2021 via non-linear explicit analysis, importing the three lattice structures as meshed bodies from nTopology. Each lattice part is placed between two rigid planes representing the upper and lower interfaces of the compression platens in compression testing. Rig compliance is negligible due to the low modulus of the photopolymer relative to steel pistons. The numerical material model corresponds to the experimentally characterized VeroCyan photopolymer used for specimen fabrication. The constitutive parameters were obtained from dedicated uniaxial tensile and compression tests performed according to ASTM D638 and ASTM D695 standards, respectively, and subsequently implemented into Abaqus through true stress–true strain plastic flow curves (details are reported in Supplementary Information Section S1). Key material elastoplastic properties defined in Abaqus include: i) Young's Modulus (E = 2238 MPa): characterizes elastic stiffness; ii) Poisson's Ratio (ν = 0.4): relates axial and lateral strain, ensuring realistic volumetric response; iii) Plastic Strain vs. Yield Stress curve: captures post-elastic behavior and hardening; iv) Elongation at break: between 10% and 25%, defines material ductility; v) Stress triaxiality: hydrostatic-to-von-Mises stress ratio, critical for ductile failure modeling; vi) Strain rate sensitivity: accounts for rate-dependent material behavior.

The constitutive behavior was modeled using an elastoplastic formulation calibrated from the experimentally obtained true stress–-true strain curves. Failure was simulated through a ductile damage criterion based on the experimentally determined failure strain and the corresponding stress-triaxiality conditions. Following damage initiation, progressive degradation of the material stiffness was introduced and complete failure was represented through element deletion. This approach enabled the simulation of localized strut rupture, damage propagation, and the progressive collapse mechanisms observed during compression testing.

Lattice structures interact via hard contact with a tangential penalty coefficient of 0.2, approximating the friction between thermoset polymers and steel [43]. Contacts between the lattice and planes are modeled. Meshes are generated in nTopology and refined through an h-refinement convergence study, performed by progressively increasing the mesh density while monitoring the global force–displacement response, peak von Mises stress, and the localization of plastic deformation within the lattice struts. Convergence was considered achieved when the variation in the monitored quantities between successive mesh refinements remained below 5%. Particular attention was dedicated to the stabilization of stress concentrations at nodal junctions and in regions prone to local buckling and shear-band nucleation. The final meshes consisted of approximately 1.8–2 million linear tetrahedral (C3D4) elements, providing a suitable compromise between computational efficiency and numerical accuracy while accurately capturing localized deformation and progressive collapse mechanisms. Further details have been provided in the Supplementary Information S.2.

2.4. Digital fabrication

Three replicas per each specimen class (*Baseline*, *Twinned*, *Optimized*) are fabricated using PolyJet 3D printing on a Stratasys J750 UV printer, employing VeroCyan™ (RGD841, Stratasys® Ltd., USA) as the photopolymer material. The process deposits liquid photopolymer droplets layer by layer onto the build platform, with each droplet instantaneously cured by UV light, ensuring precise layer solidification. The printing resolution is set to 200 µm, providing a balance between build speed and geometric fidelity. PolyJet technology enables precise control of geometry and mechanical properties, delivering high geometric accuracy, smooth surfaces, and fine feature resolution. This makes it particularly suitable for replicating complex lattice geometries, requiring strict dimensional precision, while minimizing post-processing. The printing process was performed with a nominal layer thickness of 14 µm and high-quality printing mode to maximize geometric fidelity. The specimens were fabricated with a consistent build orientation for all architectures in order to minimize variability associated with process anisotropy. Temporary SUP706 support material was automatically generated within the lattice cavities and subsequently removed using a pressurized water-jet cleaning process. Following support removal, the specimens were inspected to verify the integrity of the struts and nodal connections before mechanical testing.

2.5. Experimental analyses

Uniaxial compression testing is performed on the 3D-printed specimens using an INSTRON ElectroPuls™ machine (Instron Systems, Norwood, United States) equipped with a 10 kN load cell. Three lattice configurations, *baseline*, *twinned*, and *optimized*, are tested, with three replicas per class to ensure reproducibility.

A constant nominal strain rate of 0.005/min is applied, with a displacement limit of 20 mm, corresponding to an approximate compressive strain of 50%. Load–displacement data are continuously recorded throughout the tests, enabling quantitative assessment of the mechanical response, deformation behavior, and structural resilience of each lattice type under uniaxial compression.

To capture full-field strain distributions, Digital Image Correlation (DIC) is employed using a Q-400 system equipped with dual 12 MP cameras (LIMESS GmbH, Krefeld, Germany), operating at a sampling frequency of 1 Hz. Specimens are prepared with a high-contrast speckle pattern, consisting of black dots on a white-painted background, to optimize correlation accuracy [74]. Strain fields, including equivalent von Mises strain, are analysed using Instra 4D v4.6 software (Dantec Dynamics A/S, Skovunde, Denmark), providing spatially resolved measurements of local deformation and enabling detailed investigation of strain localization, load redistribution, and failure mechanisms across the lattice structures. In detail, the DIC analysis was performed on the central region of the specimens to minimize boundary artefacts during compression. Correlation was conducted using a subset size of 29 × 29 pixels and a step size of 7 pixels, selected to provide a suitable compromise between spatial resolution and correlation stability during large deformation. Additional details regarding the experimental setup and DIC parameters are provided in the Supplementary Information (Section S3).

For all architectures, compression is applied along the vertical direction of the specimen. In the twinned and optimized configurations, the twin boundary is located along the central symmetry plane, providing the reference frame for the development of the observed shear-band patterns.

The effective in-plane Poisson's ratio of the lattice architectures was estimated from the DIC strain fields according to:

$$\nu_{eff} = -\frac{\varepsilon_{trans}}{\varepsilon_{axial}} \tag{6}$$

where ε_{trans} and ε_{axial} represent the average transverse and axial strains measured within the central region of interest. The evaluation was performed during the initial homogeneous deformation regime, prior to the onset of pronounced strain localization.

2.6. Quantification of the sequential design amplification

To quantitatively evaluate the effectiveness of the proposed sequential bio-inspired design strategy, a Sequential Energy Amplification Factor (SEAF) was introduced. Since the primary objective of the study is the simultaneous enhancement of strength and deformation capacity, the absorbed mechanical energy up to peak load was selected as the representative performance metric.

The absorbed energy was estimated as the area under the force–displacement curve up to the maximum load:

$$U = \int_0^{\delta_{max}} F\, d\delta \tag{7}$$

where F is the compressive force and δ is the displacement.

The Sequential Energy Amplification Factor was then defined as:

$$SEAF = \frac{U_{OPT} - U_{TWIN}}{U_{TWIN} - U_{BASE}} \tag{8}$$

where U_{BASE}, U_{TWIN}, and U_{OPT} denote the energy absorbed by the baseline, twinned, and optimized architectures, respectively.

This metric quantifies how much the topology optimization stage amplifies the energy gain initially introduced by twinning. A value greater than 1 indicates that the second design stage contributes more than the first design stage.

3. Results and discussion

This study aims at engineering architected metamaterials capable of overcoming the strength-ductility trade-off that characterizes most lattice-based cellular solids. Conventional strut-based architectures, such as the FCC and BCC lattices, typically exhibit stretching-dominated deformation and fail catastrophically once local buckling or brittle fracture initiates, thereby limiting their energy absorption capacity and post-yield resilience [1–3]. This mechanical limitation parallels that of crystalline solids in which plastic deformation is restricted to dislocation slip, resulting in localized shear and premature fracture. To transcend these constraints, the present work adopts a bio-inspired strategy that translates the paradigm of twinning-assisted plasticity into the mesoscale design of cellular lattices. By embedding synthetic TBs into the lattice geometry, it is hypothesized that stresses can be redistributed across multiple load paths, thereby delaying localization, activating alternative deformation mechanisms, and enhancing energy dissipation.

3.1. Metamaterial design: A bio-inspired evolutionary approach

The evolutionary design framework adopted in this study is inspired by the progressive evolution of plants, in which mechanical competence emerges through successive adaptations driven by functional necessity. This stepwise evolutionary logic provides a conceptual lens through which the mechanical response of the investigated lattices can be interpreted, as schematically illustrated in Fig. 2a.

The mechanical significance of the two evolutionary steps, the biological analysis and target metrics are detailed in Table 2.

The *baseline* FCC lattice exhibits a relatively isotropic elastic response but fails through highly localized strut buckling, leading to rapid post-peak strength degradation. This behavior reflects a lack of intrinsic mechanisms for stress delocalization, resulting in limited ductility and damage tolerance. The introduction of architectural twinning (*twinned* structure) constitutes the first evolutionary adaptation and produces a clear qualitative change in deformation behavior. By embedding a mesoscale twin boundary through mirroring of the lattice orientation, stresses are redistributed across the structure, delaying localization and promoting a more distributed deformation mode. This behavior is analogous to the role of vascular tissues in plants and to deformation twinning in crystalline metals. While the twinned lattice exhibits enhanced ductility and a more stable post-yield response compared to the baseline FCC configuration, strength remains limited by stress concentrations within the struts, indicating that twinning alone is insufficient to fully optimize mechanical performance. A second evolutionary refinement is achieved through topology optimization (*optimized* structure) applied directly to the twinned unit cell, paralleling the emergence of lignin in plant evolution, which reinforced existing vascular architectures rather than replacing them. The optimization is formulated to minimize the maximum von Mises stress while preserving lattice periodicity and manufacturability, with a target material removal fraction of 80% of the initial design space mass and a minimum strut diameter of 1 mm (Fig. 2b). Convergence is achieved after 47 iterations, resulting in a refined strut geometry characterized by redistributed load paths and suppressed stress concentrations. Unlike the straight members of the *baseline* and *twinned* FCC lattices, the *optimized* struts exhibit variable cross-sections and curvilinear trajectories, which are known to improve buckling resistance and energy absorption. The final *optimized* lattice is presented in Fig. 2b on the right, illustrating both shell-free and shell-enclosed configurations.

Herein, the evolutionary analogy with plant development provides a useful interpretive framework, highlighting how successive adaptations address increasingly stringent mechanical requirements and ultimately lead to a more resilient and efficient structural system.

3.2. Analytical framework for mass-invariant metamaterial optimization

The analytical framework described in Section 2.2 confirms that the three investigated architectures are designed under approximately mass-invariant conditions. The relative density of both the baseline and optimized unit cells is found to be 0.2034, while the measured masses of the fabricated specimens remain within a narrow range (10.9–11.6 g).

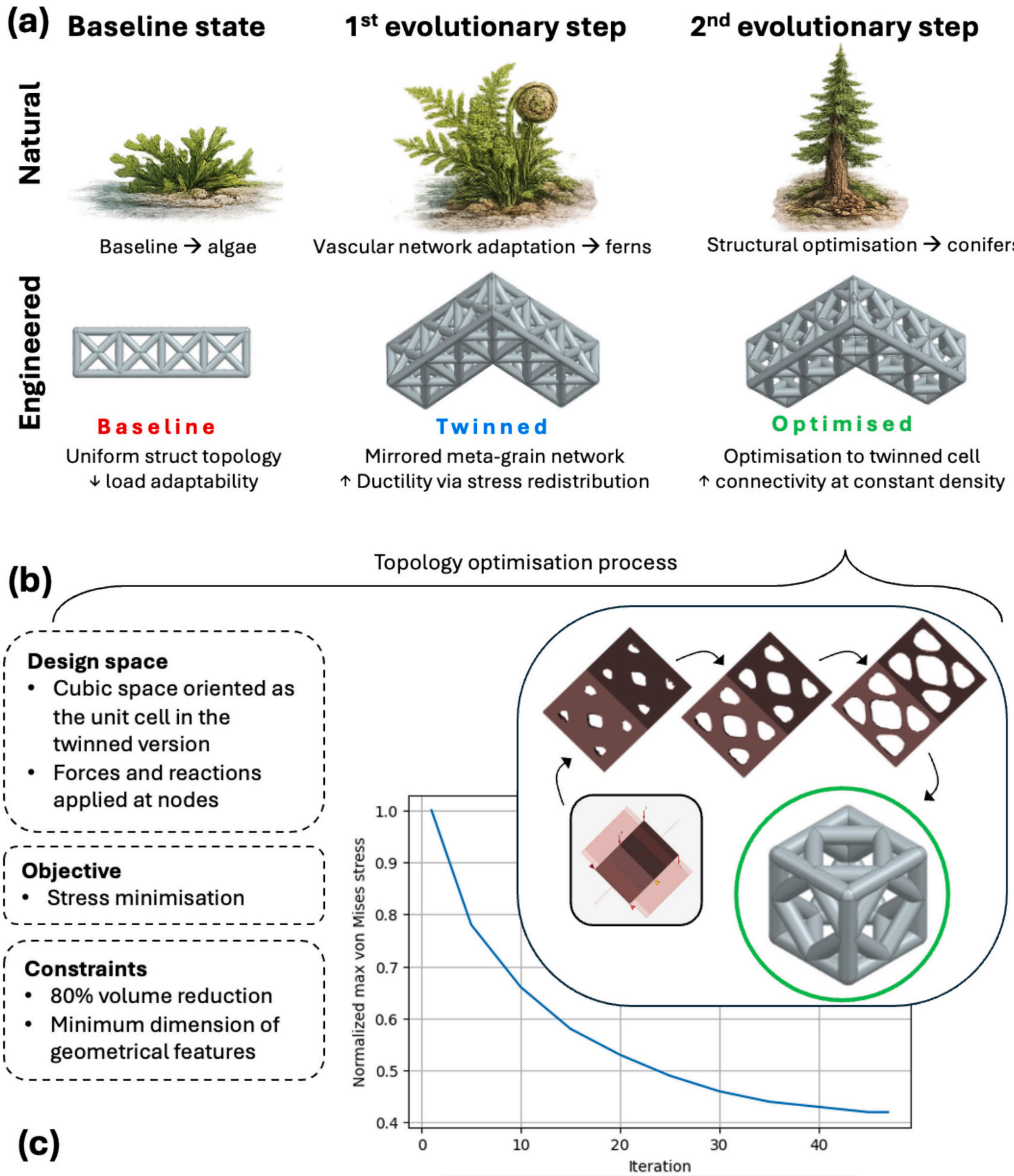

	TWINNED	OPTIMIZED
RELATIVE DENSITY [%]	20.4	20.4
CONNECTIVITY [nodes/unit cell]	4	7
CRITICAL LOAD [N/unit cell]	229	302
TOTAL MASS [g]	16.6	16.4

Fig.2. Bio-inspired evolutionary design framework for *twinned* and *optimized* architected lattices. (a) Schematic of the hierarchical, evolution-driven design strategy in which principles observed in biological materials are translated into architected metamaterials. The top row presents the biological analogy, progressing from algae (soft, non-load-bearing tissues) to vascular plants (stress redistribution through internal transport networks) and finally to woody plants, where lignification provides enhanced structural resistance. The bottom row shows the corresponding evolution in lattice architectures, from a *baseline* FCC lattice to a *twinned* configuration incorporating a central mirror-symmetric boundary, and ultimately to an *optimized* twinned lattice. (b) Details of the topology optimization workflow applied to the *twinned* unit cell, including the definition of the design domain, loading and boundary conditions, objective function (stress minimization), and geometric constraints. The inset on the right reports the evolution of the normalized objective function throughout the 47 optimization iterations, illustrating the convergence of the SQP-based optimization procedure toward the final design. (c) Comparison between *twinned* and *optimized* unit cells in terms of relative density, connectivity, critical load and total mass.

Table 2
Mechanical significance of the evolutionary design framework.

Evolutionary step	Biological analogy	Biological role	Architectural modification	Target mechanical metrics
Step 1: Baseline → Twinned	Development of vascular tissues	Enable efficient transport and redistribution of water and nutrients throughout the plant, improving adaptability and preventing localized resource depletion	Introduction of a twin boundary and mirrored *meta*-grains	Stress redistribution, delayed strain localization, shear-band regulation, deformation capacity
Step 2: Twinned → Optimized	Development of lignified tissues	Provide structural reinforcement, improve load-bearing capability, and enable plants to sustain larger mechanical loads	Topology optimization of the twinned unit cell	Connectivity, critical load, stress-transfer efficiency, structural stability

Post-fabrication mass measurements further confirm the validity of the mass-invariant design strategy, ensuring that the observed differences in mechanical response originate primarily from architectural modifications rather than variations in material volume (Supplementary Information S.4).

Maintaining equivalent relative density is particularly important in architected materials because stiffness, strength, and energy absorption are strongly influenced by the amount of material contained within the structure. By preserving both mass and relative density, the comparison between the baseline, twinned, and optimized architectures could be focused on the influence of geometry, connectivity, and deformation mechanisms.

Connectivity analysis reveals substantial differences between the baseline and optimized unit cells. The baseline FCC architecture exhibit a connectivity index of 4, whereas the optimized unit cell reaches a connectivity index of 7, corresponding to a 75% increase in connectivity. This increase reflects the introduction of additional nodal interconnections and a greater number of available load-transfer pathways throughout the unit cell.

From a mechanical perspective, the increase in connectivity reduces the dependence of the structure on a limited number of highly loaded members and promotes a more distributed transfer of forces. Consequently, stresses can be redistributed through multiple structural pathways, reducing stress concentrations and delaying the formation of localized failure regions. This behavior is consistent with previous studies [31,75] showing that highly connected lattice architectures generally exhibit enhanced structural robustness, improved damage tolerance, and greater resistance to instability-driven collapse.

The influence of topology optimization on structural stability is further assessed through simplified beam-model analyses. The baseline and optimized unit cells exhibit critical loads of approximately 229 N and 302 N, respectively, corresponding to a 32% increase in critical load. This result indicates that the optimized architecture can sustain substantially larger loads before the onset of instability and therefore possesses greater resistance to buckling-induced failure.

The corresponding buckling and stress analyses are reported in Fig. 3a,b. The first-mode buckling shapes shown in Fig. 3a demonstrate the improved structural stability of the optimized architecture, which exhibits a noticeably higher load multiplier than the baseline configuration. This improvement is not solely a consequence of enhanced connectivity but also results from the modified orientation of the load-carrying members and the redistribution of material within the unit cell, which together generate more favourable stress-transfer pathways.

The von Mises stress distributions reported in Fig. 3b provide additional insight into the mechanical consequences of these architectural modifications. When loaded up to their respective critical conditions, the optimized unit cell develops higher local stresses than the baseline configuration. This observation indicates a change in the governing failure mechanism. While the baseline FCC architecture fails primarily through buckling of axially loaded members, which is characteristic of stretching-dominated systems, the optimized architecture exhibits a transition toward a bending-dominated deformation regime in which yielding becomes the dominant failure mechanism before global instability develops.

This transition is particularly important because it provides a mechanistic explanation for the enhanced deformation capacity observed experimentally. Rather than concentrating deformation within a small number of vertical struts, the optimized architecture distributes stresses across a larger number of interconnected members, enabling progressive deformation and delaying catastrophic collapse.

Here, the analytical framework highlights three key consequences of topology optimization: (i) preservation of relative density and mass, enabling an unbiased comparison among architectures; (ii) a 75% increase in connectivity, promoting more efficient stress redistribution and multiple load-transfer pathways; and (iii) a 32% increase in critical load, indicating enhanced resistance to instability.

It should be noted that the analytical framework presented in Fig. 3 is intended to evaluate the influence of topology optimization at the unit-cell level. Since the Twinned architecture employs the same FCC unit cell as the baseline configuration and differs only through the introduction of a twin boundary at the lattice scale, its mechanical contribution cannot be captured by a simplified unit-cell beam model. The effect of twinning is therefore assessed through the full-lattice finite-element simulations and experimental analyses presented in the following sections.

3.3. *Numerical results*

The numerical analyses provide a comprehensive insight into the stress evolution, plastic deformation, and failure mechanisms governing the mechanical response of the base, twinned, and optimized lattice architectures.

To facilitate comparison among the investigated architectures, the principal structural descriptors governing their mechanical response are summarized as follows. The baseline FCC lattice is characterized by a conventional FCC arrangement with a unit-cell orientation aligned with the specimen boundaries and a nominal strut diameter of 0.95 mm. The twinned lattice introduces a central twin boundary and a 45° unit-cell orientation while maintaining the same relative density. The optimized lattice preserves the twin-boundary configuration and relative density of the twinned architecture, but exhibits enhanced nodal connectivity (approximately + 75%) and an increased critical load (approximately + 32%) resulting from the topology optimization process. These architectural features strongly influence the stress redistribution pathways, deformation modes, and failure mechanisms observed in the finite-element simulations.

Time-resolved contour plots of the von Mises stress, extracted at selected simulation steps, reveal that each structure activates distinct load-bearing mechanisms as deformation progresses:

***i) Stage I – Linear elastic response and topology-controlled stress partitioning*.**

During the initial loading regime, all configurations exhibit a predominantly linear elastic response. The von Mises stress contours (Fig. 4, Stage I) reveal that stress partitioning is strongly governed by unit-cell topology and strut orientation. In the *baseline* lattice, stress is primarily concentrated within vertical struts aligned with the loading axis (see red arrows), consistent with a stretching-dominated load transfer mechanism. In contrast, the *twinned* lattice redistributes stress toward struts located on the unit-cell faces adjacent to the twinning plane (see light blue arrows), while the *optimized* lattice engages inclined struts

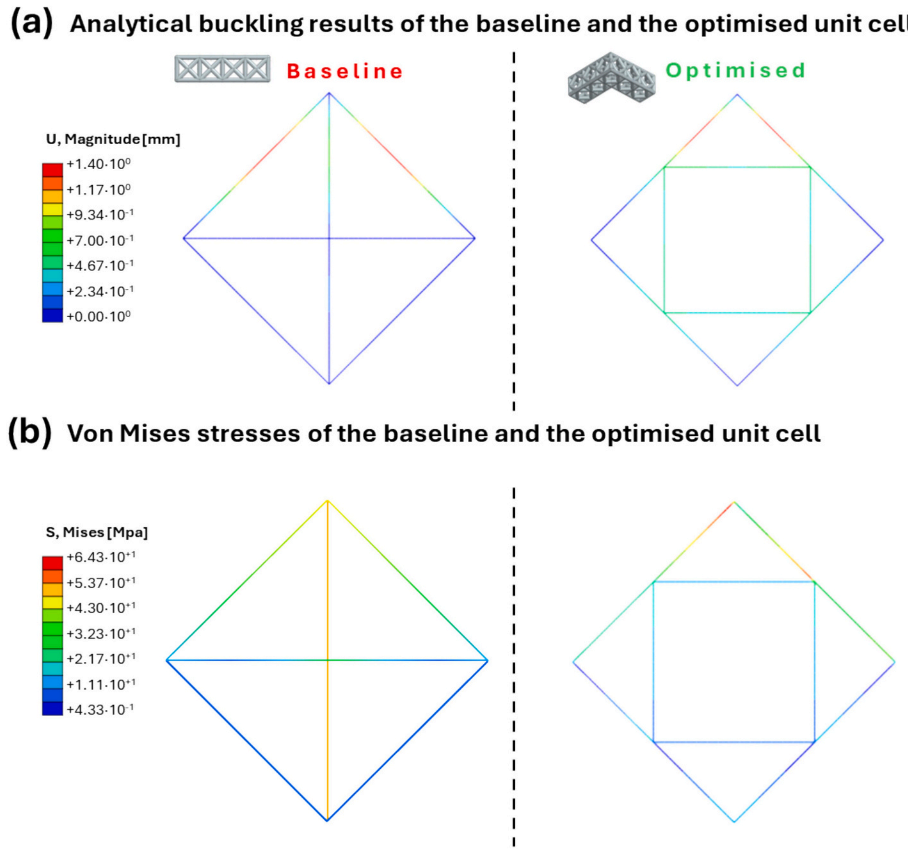

Fig.3. Buckling and stress-based failure assessment of the *baseline* and *optimized* unit-cell frame models. (a) Linear perturbation buckling analysis of the *Baseline* (left) and *Optimized* (right) unit cells, reported as the first-mode buckling shapes and corresponding load multipliers. (b) Von Mises stress fields [MPa] computed by applying to each unit cell its respective buckling load.

aligned along preferential crystallographic directions. This redistribution reflects an early activation of multiple load paths enabled by increased nodal connectivity and geometric anisotropy, despite identical relative density across all architectures.

ii) Stage II – Plastic instability and shear-band nucleation

With increasing compressive displacement, localized stress amplification triggers the onset of plastic deformation (Fig. 4, Stage II), captured by the emergence and growth of equivalent plastic strain (PEEQ). In the *baseline* lattice, plasticity initiates nearly simultaneously in vertically oriented struts and rapidly localizes within a single crystallographic plane normal to the loading direction, promoting synchronized strut yielding and limited lateral stress redistribution (see red arrows). Conversely, the *twinned* and *optimized* lattices exhibit delayed plastic initiation and a markedly more distributed plastic strain field. Yielding occurs in struts with combined axial and transverse components, leading to the nucleation of inclined shear bands (highlighted with ellipses). Importantly, these shear bands develop symmetrically with respect to the twinning plane, indicating that the mirror-symmetric architecture imposes a geometric constraint on strain localization and governs the preferred deformation modes, as highlighted by the PEEQ contours (Fig. 5).

***iii) Stage III – Progressive damage accumulation and macroscopic collapse*.**

Further loading leads to the accumulation of plastic damage and eventual strut failure, identified by element deletion and local stress relaxation (Fig. 4, Stage III). In the *baseline* lattice, strut rupture occurs almost concurrently within the same crystallographic plane, resulting in a rapid degradation of load-carrying capacity and an abrupt global collapse. In contrast, the *twinned* and *optimized* architectures undergo a progressive failure process, characterized by damage propagation across multiple planes prior to the formation of a dominant shear band spanning the entire specimen. This distributed failure mechanism delays macroscopic collapse and enhances structural stability. At the final stage, a sharp reduction in stress indicates complete unloading, corresponding to the inability of the remaining strut network to sustain further compressive loading.

Herein, the numerical analyses demonstrate that the introduction of twinning fundamentally alters the deformation sequence by promoting stress redistribution and symmetry-controlled shear localization, while subsequent geometric optimization further suppresses localized instabilities. The combined effect shifts the governing failure mode from plane-dominated, stretching-controlled rupture in the base lattice to a progressive, shear-driven plastic collapse in the *twinned* and *optimized* architectures, thereby significantly enhancing mechanical robustness under compression.

To facilitate interpretation of the numerical results, the principal structural descriptors of the three architectures and their influence on the observed deformation mechanisms are summarized in Table 3.

3.4. Experimental results

Uniaxial compression tests are conducted on the three metamaterial configurations, with deformation monitored in situ through DIC. Representative images of the specimens during loading are reported in Fig. 6.

The *baseline* lattice exhibits a limited deformation regime and brittle failure localized along a distinct crystallographic plane. As shown in Fig. 6a on the left, the failure plane is clearly identified on the specimens, corresponding to a preferential alignment of struts. This observation is confirmed by the strain field obtained via DIC, where a sharp

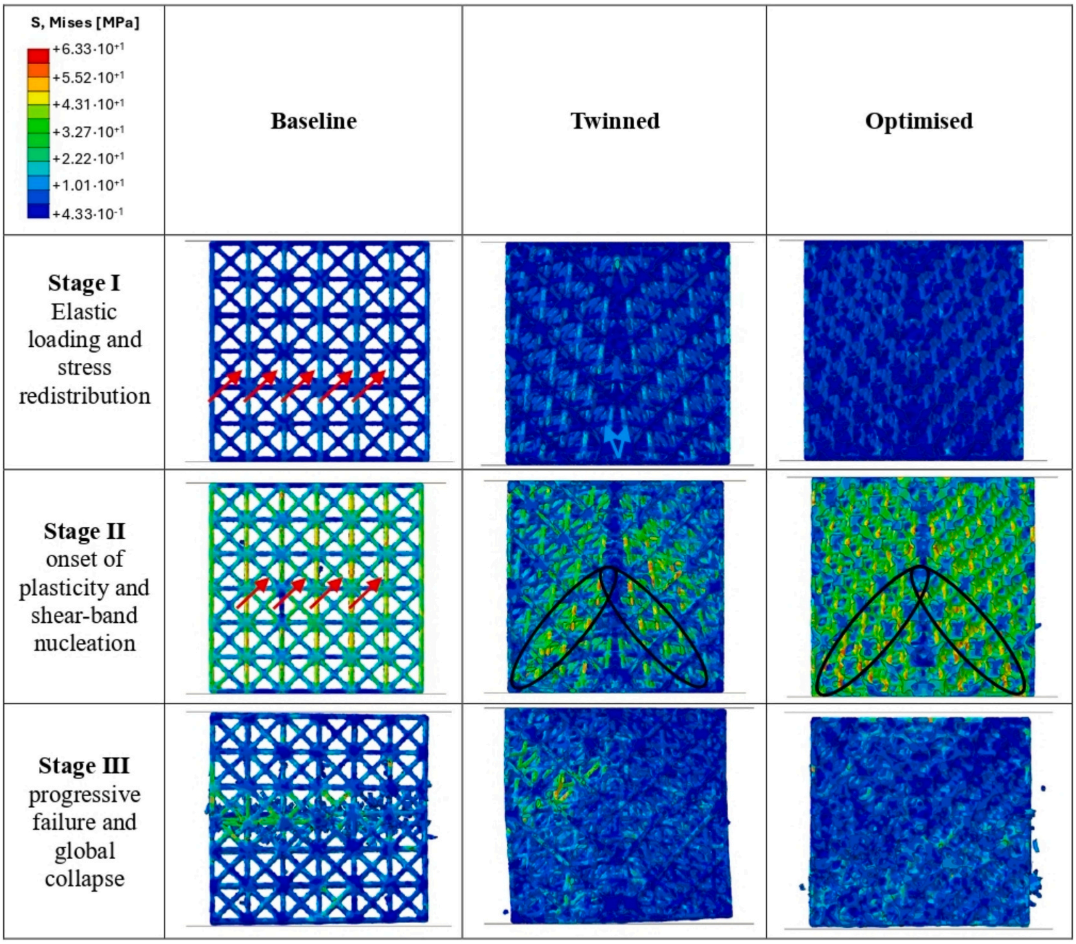

Fig. 4. Contour plots for the von Mises stresses at progressively increasing displacement steps (i.e. Stage I: elastic loading, Stage II: onset of plasticity, Stage III: failure).

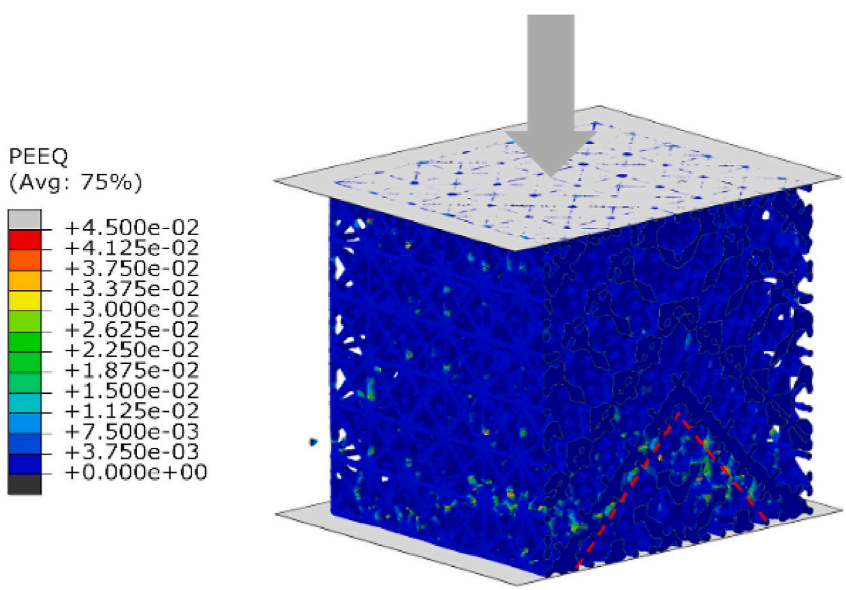

Fig. 5. Equivalent plastic strain (PEEQ) contours of the *optimized* structure. The compression direction is vertical (grey arrow), while the twin boundary is located along the central symmetry plane of the specimen. The presence of shear bands is highlighted with dashed red lines.

gradient confirms the onset of localized deformation immediately prior to collapse. The utility of DIC is particularly evident in this context: given the sudden fracture of the baseline lattice, conventional strain measurement methods would have been insufficient to capture the transient deformation events. The DIC analysis further reveals severe strain localization in the vertical struts, resulting in abrupt, layer-by-

Table 3
Structural characteristics of the investigated architectures and their expected influence on the mechanical response.

Architecture	Key structural feature	Quantitative parameter (validation of evolutionary step metrics)	Expected mechanical effect	Observed numerical response
Baseline	Conventional FCC arrangement	Relative density = 0.2034; strut diameter = 0.95 mm	Load mainly transferred through vertical struts	Strong stress localization in vertical members; stretching-dominated deformation; buckling-controlled failure
Twinned (evolutionary step 1)	Introduction of a central twin boundary	Twin boundary present; unit-cell orientation = 45°; relative density = 0.2034	Stress redistribution across multiple deformation paths; delayed localization	Symmetric shear-band formation; more distributed stress field; increased deformation capacity
Optimized (evolutionary step 2).	Topology-optimized unit cell combined with twin boundary	Relative density = 0.2034; connectivity increase ≈ 75%; critical load increase ≈ 32%; strut diameter = 1 mm	Enhanced load transfer, reduced stress concentrations, activation of multiple deformation pathways	Distributed stress field; stable shear-band development; bending-dominated deformation; delayed failure and higher peak load

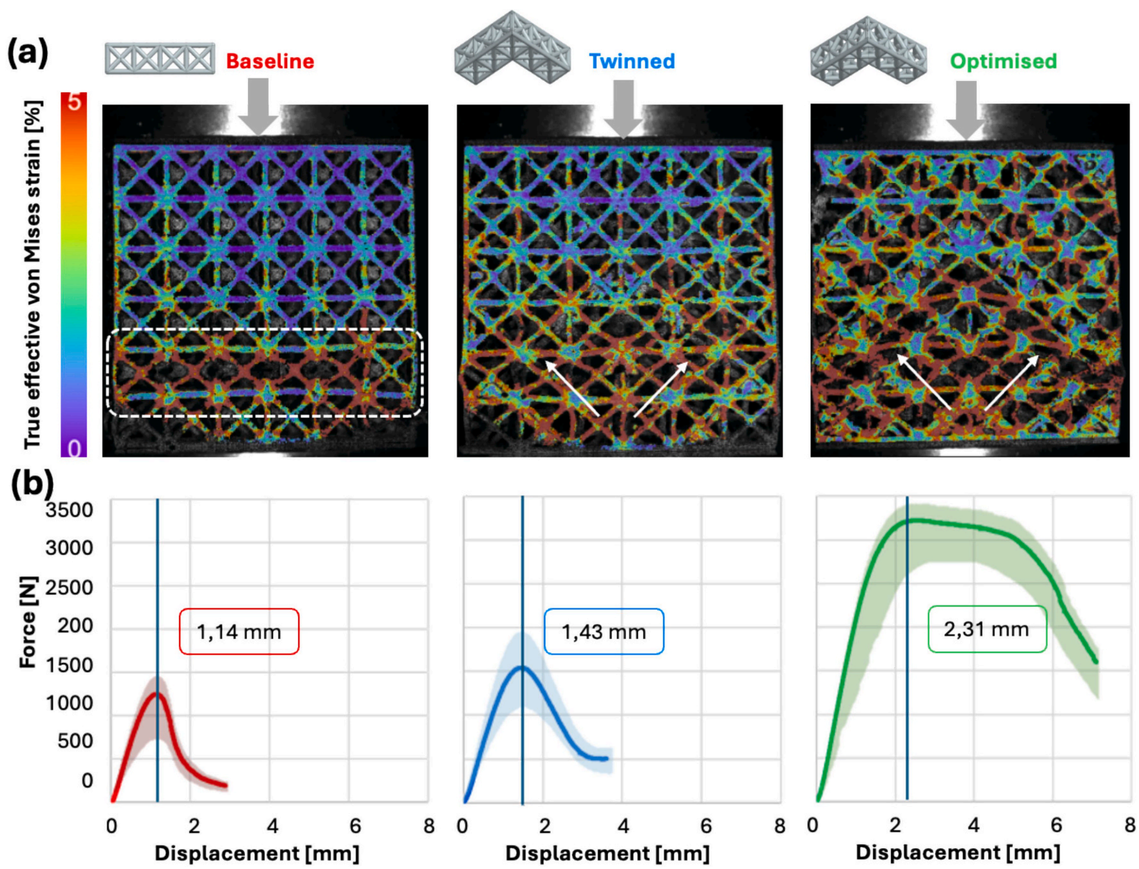

Fig.6. Experimental compression response of *baseline*, *twinned*, and *optimized* lattice architectures. (a) Digital Image Correlation (DIC) maps in correspondence of the maximum load of the three classes during uniaxial compression, showing the spatial distribution of true effective von Mises strain (%) at comparable deformation states. (b) Corresponding force–displacement curves obtained from compression tests for the three architectures until fracture. The reported displacement values are corrected for machine compliance. Solid lines represent the mean response, while shaded regions indicate standard deviations. Rectangles highlight the displacement at peak load, illustrating the progressive increase in both peak force and deformation capacity from baseline to twinned and optimized designs. The compression direction is vertical in all specimens (grey arrow). For the twinned and optimized architectures, the twin boundary acts as a symmetry plane governing the observed deformation and shear-band development.

layer collapse and highlighting the brittleness of the base design.

The introduction of twinning within the *twinned* unit-cell architecture markedly altered the failure mechanism. As shown in Fig. 6a in the centre, the redistribution of struts within the volume facilitated a more gradual failure response, with stress initially dispersed across multiple planes before concentrating along shear bands. The corresponding DIC maps confirm the progressive accumulation of strain in specific orientations (white arrows). This response is consistent with the concept of twinning as an adaptive design strategy, in which redistribution of stresses mitigates abrupt fracture and enhances energy absorption. While the twinned lattice demonstrated higher load-bearing capacity and more homogeneous strain distribution than the base lattice, the DIC analysis indicated that plastic deformation remained relatively limited, with shear bands less pronounced than in highly ductile systems.

In contrast, the *optimized* lattice displayed a distinct mechanical behavior characterized by extended plasticity and pronounced shear banding. During loading, significant deformation was visible even macroscopically, with DIC confirming the development of a well-defined shear band spanning the specimen volume (Fig. 6a on the right). The *optimized* lattice sustained higher strains prior to collapse, exhibiting the longest plastic phase among the tested structures and achieving the highest failure load. This delayed failure suggests that the optimization process effectively promoted stress redistribution and enhanced energy dissipation by guiding load paths through reoriented and more highly connected truss networks (white arrows). As a result, the *optimized* lattice exhibited improved toughness and superior resistance to catastrophic fracture.

The mechanical response is quantitatively summarized in the force–displacement curves reported in Fig. 6b. The *baseline* lattice showed multiple peaks associated with sequential collapse of vertical struts in individual layers, consistent with brittle layer-by-layer failure. This stepwise collapse was significantly attenuated in the *twinned* and *optimized* lattices, which instead exhibited smoother curves reflecting alternative failure modes. In these cases, the absence of discrete layered failure was accompanied by strain-hardening behavior arising from increased strut interactions and load redistribution. The maximum failure load increased from approximately 1000 N in the *baseline* structure to $\sim$ 1500 N in the *twinned* lattice and $\sim$ 3500 N in the *optimized* version, while the displacement at failure increased from $\sim$ 1.0 mm (*baseline*) to $\sim$ 1.5 mm (*twinned*) and $\sim$ 2.5 mm (*optimized*). These trends confirm a progressive improvement in both strength and ductility from the base to the optimized design.

Finally, Fig. 6 gives indication about the first fracture event, highlighting the transition in failure mechanisms. In the *baseline* lattice, strain localization is confined to vertical struts, leading to highly brittle fracture. In the *twinned* lattice, load sharing across non-axially aligned struts improves stability, though ductility gains remained moderate. In the *optimized* lattice, the emergence of stable shear bands facilitates large plastic deformation, correlating with enhanced toughness and gradual failure. These results validate the hypothesis that sequential, bio-inspired modifications, twinning followed by topology optimization, progressively increase both the load-bearing capacity and ductility of architected lattices by promoting controlled stress redistribution and delaying catastrophic collapse. The observed scatter of Fig. 6b is attributed primarily to manufacturing-related factors, including dimensional tolerances, local variations in photopolymer curing, and minor geometric imperfections associated with the additive-manufacturing process.

To quantitatively assess the effectiveness of the proposed sequential design framework (Baseline → Twinned → Optimized), the absorbed energy up to peak load was estimated from the experimental force–displacement curves. The baseline, twinned, and optimized architectures exhibited absorbed energies of approximately 500, 1125, and 4375 N·mm, respectively. Based on these values, the Sequential Energy Amplification Factor (SEAF) was calculated as 5.2. This result indicates that topology optimization amplifies the energy gain introduced by twinning by more than fivefold, highlighting the effectiveness of combining deformation-regulating twin boundaries with topology-driven load-path optimization.

Additionally, the effective Poisson's ratios obtained from the DIC measurements were computed and these results in 0.28 ± 0.04, 0.17 ± 0.03, and 0.08 ± 0.03 for the *Baseline*, *Twinned*, and *Optimized* architectures, respectively. The progressive reduction in Poisson's ratio indicates decreasing lateral expansion and is consistent with the increasing influence of stress redistribution, internal rotation, and bending-dominated deformation mechanisms. [76,77].

These values are consistent with the positive effective Poisson's ratios commonly reported for twinning-inspired and conventional FCC-based lattice architectures and differ from the negative Poisson's ratios observed in auxetic metamaterials [76,77]. This comparison confirms that the improved mechanical performance of the present architectures originates from stress-delocalization and connectivity-enhancement mechanisms rather than from auxetic kinematics.

It should be noted that the force–displacement curves shown in Fig. 6 (b) correspond to the complete experimental response up to specimen fracture and therefore capture the entire deformation process, including the post-yield regime and final failure stage. As a result, the area under the curves can be interpreted as a measure of the energy absorbed during deformation. A progressive increase in absorbed energy is observed from the baseline to the twinned and optimized architectures, reflecting the combined improvement in load-bearing capacity and deformation capability. The optimized architecture exhibits the largest absorbed energy owing to its higher peak load and delayed failure.

3.5. Deformation and strength gains: Experimental and numerical comparisons

The combined experimental–numerical investigation highlights a progressive, quantifiable improvement in both deformability and load-bearing capacity as the lattice architecture evolves from the base geometry through the twinned variant to the fully optimized configuration.

The validation of the numerical framework was performed through a multi-level comparison between simulations and experiments. Agreement was assessed not only through global mechanical metrics such as peak load and deformation capacity, but also through comparison of the strain-localization patterns obtained from DIC with the corresponding PEEQ distributions predicted numerically, as well as through the observed deformation and failure mechanisms, including shear-band formation, stress redistribution, and progressive collapse. This validation strategy was adopted to assess both the global response and the underlying physical mechanisms governing lattice deformation.

FE analysis contour maps (Fig. 7a on the left) and DIC strain fields (Fig. 7a on the right) demonstrate excellent qualitative alignment in all three architectures. In both experiment and simulation, the dominant shear bands in the *optimized* lattice follow the same inclined planes, confirming that the numerical model captures the critical stress trajectories responsible for failure initiation. In detail: i) *Baseline* lattice: brittle, layer-wise collapse along horizontal planes; ii) *Twinned* lattice: shear bands inclined at $\sim 45^\circ$, signifying redistribution of stresses across twin boundaries; iii) *Optimized* lattice: continuous, well-developed diagonal shear bands indicating extensive plastic accommodation.

The correspondence of these strain paths validates the numerical approach as a reliable predictive framework for assessing comparative mechanical behavior.

Compression tests show a clear gain in both deformation and strength [%] in the *twinned* and *optimized* lattice with respect to the *baseline*, that are quantified in Fig. 7b.

These data highlight two key trends: ii) Twinning as an intermediate enhancer: the addition of twin boundaries introduces new load paths and delays local buckling, enabling a modest but statistically significant increase in both ductility and strength without sacrificing stiffness; ii) Topology optimization as a transformative step: the optimized geometry nearly doubles the experimental failure strain and more than doubles the maximum sustainable load. This net improvement arises from a global redistribution of stresses and an increase in nodal connectivity, which together suppress early localization and permit extensive plastic accommodation.

It is important to note that twinning and topology optimization play fundamentally different roles within the proposed design framework. Twinning primarily acts as a deformation-regulating mechanism by promoting stress delocalization and delaying strain localization, as evidenced by the emergence of symmetric shear bands and the increased deformation capacity of the twinned lattice. In contrast, topology optimization mainly enhances strength by improving load transfer and reducing stress concentrations. Therefore, the larger quantitative gains observed in the optimized architecture should not be interpreted as diminishing the contribution of twinning; rather, they indicate that topology optimization is able to exploit and amplify the deformation pathways introduced by the twinned architecture.

Although the optimization objective was solely stress minimization, the resulting architecture exhibited increased connectivity and modified load-transfer pathways, which promoted a transition toward a bending-dominated deformation regime. These mechanisms provide a physical

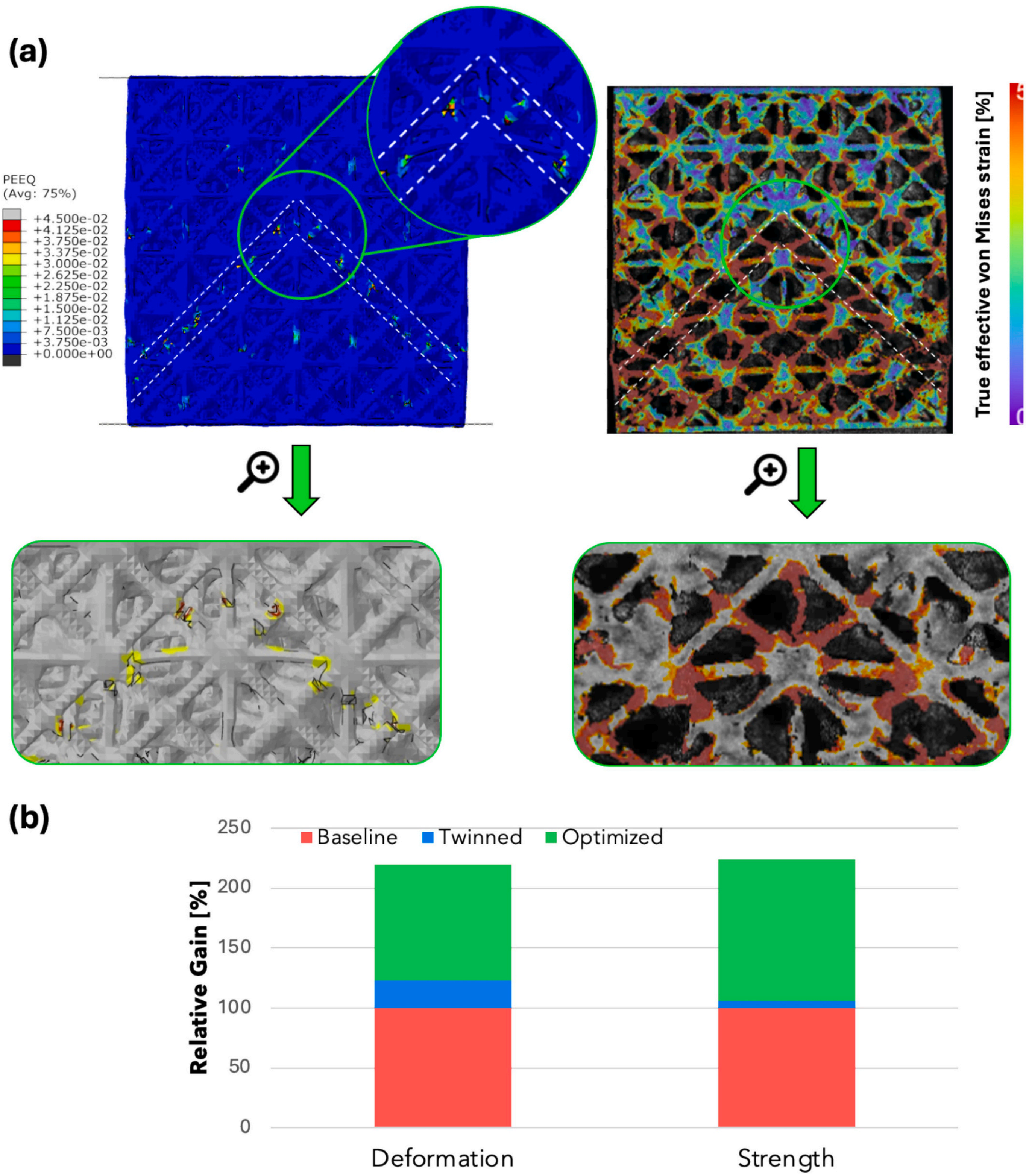

Fig.7. Comparison between numerical and experimental results related to the strain localization in the *optimized* lattice under compression. (a) Numerical and full-field Digital Image Correlation (DIC) maps showing the spatial distribution of strains. Dashed lines indicate the formation of inclined shear bands, while green circles highlight regions of interest where strain localization initiates (magnified views are reported in the green boxes). (b) Quantitative decomposition of the deformation and strength gains [%] in the *twinned* and *optimized* lattice with respect to the baseline.

explanation for the improvements in deformation capacity and energy absorption observed experimentally.

Micro-mechanistic interpretation

The *twinned* lattice promotes stress delocalization: non-axially aligned struts share the applied compressive load, so that strain energy accumulates gradually rather than catastrophically. This reduces the severity of the first fracture event and creates a smoother force–displacement curve.

In the *optimized* lattice, the combination of increased connectivity and strategically reoriented struts enhances bending-stretching coupling, which is well known to elevate both the initial stiffness and the energy absorption capacity of lattice metamaterials. DIC shows extensive shear-banding before global failure, a hallmark of pseudo-ductile behavior where plastic deformation proceeds through progressive cell collapse and localized rotations rather than abrupt brittle fracture.

Design implications

The nearly twofold increase in ductility and more than doubling of strength achieved by the *optimized* lattice underscores the effectiveness of a multi-stage design strategy: firstly, crystallographic twinning introduces alternate load paths and enhances damage tolerance; secondly, topology optimization exploits these added degrees of freedom to channel stresses along energetically favourable routes.

This adaptability-driven paradigm is broadly applicable to architected materials intended for load-bearing applications where energy absorption, fail-safe deformation, and predictable failure planes are critical, such as biomedical scaffolds, aerospace crash absorbers, or protective mechanical metamaterials.

3.6. Potentialities, limitations, engineering challenges and future opportunities

This work demonstrates that combining crystallographic-inspired twinning with topology optimization provides a powerful pathway for tailoring the mechanical response of architected lattices, but it also highlights key boundaries in both design and modeling that inform future developments.

The experimental and numerical campaign confirms the initial theoretical expectation of substantial ductility enhancement in lattices with twin boundaries, with measured increases ranging from ≈20 % consistent with previous studies [26,28], to > 90 % with our designed evolutionary-based optimization process. The *twinned* architecture redistributes stresses over multiple planes, delaying localization and suppressing abrupt fracture, while retaining a predominantly stretching-dominated load path. In contrast, the *optimized* lattice exhibits a bending-dominated unit-cell response, as illustrated in Fig. 6, which facilitates larger rotations and plastic hinge formation. This shift in deformation mechanism produces an extended plastic regime and superior energy absorption relative to the twinned design. Strength gains are equally significant. The *optimized* lattice reaches a 118 % higher peak load than the base design, a result anticipated by the topology-optimization strategy and supported by beam-model analyses and finite-element simulations. High nodal connectivity, well documented to correlate positively with peak strength in cellular materials [31], further substantiates the performance increase. Herein, these findings underscore the design flexibility of lattice metamaterials, where geometric motifs (twin boundaries, nodal connectivity, strut orientation) can be systematically tuned to balance stiffness, ductility, and energy absorption. Such tunability opens application spaces ranging from lightweight crash absorbers and impact-protective gear to biomedical scaffolds, where controlled failure and high energy dissipation are critical.

A key aspect of the proposed methodology is that the investigated architectures represent successive stages of a bio-inspired evolutionary design process rather than independent parametric variations. Consequently, the optimized architecture differs from the twinned lattice through multiple interacting modifications, including enhanced connectivity, altered stress-transfer pathways, and a transition toward a bending-dominated deformation regime. The purpose of the study is therefore to evaluate the cumulative effect of these adaptations when applied to a twinned architecture, rather than to isolate each parameter independently. Future work could investigate additional architectures, such as an optimized FCC lattice without twin boundaries or architectures with systematically controlled connectivity, to quantitatively separate the individual contributions of twinning, connectivity, and deformation mode.

Despite these achievements, some limitations temper the current framework. The polymer used (VeroCyan) exhibits noticeable plasticity, enabling large strut deflections and self-interaction that enhance ductility beyond what a brittle resin would show. A more brittle SLA-printed resin could isolate geometric from material contributions, revealing the pure effect of stress delocalization. Conversely, applications requiring energy absorption may benefit from the current material's capacity for plastic deformation and strain hardening. Minor defects inherent to additive manufacturing introduce variability in failure initiation (e.g., layer-to-layer discrepancies in the base lattice) and can influence local stress concentrations. Higher-resolution printing or in-situ process monitoring would improve reproducibility and model–experiment fidelity. Additionally, although three specimens were tested for each architecture in the present study, which is consistent with common practice in experimental studies of architected materials, larger sample populations would further strengthen the statistical significance of the observed trends. Nevertheless, the differences in mechanical performance between the investigated architectures are substantially larger than the experimental variability observed among replicas. A further limitation concerns the finite size of the investigated specimens, which consisted of approximately $6 \times 6 \times 6$ unit cells and therefore cannot be considered representative volume elements in the strict homogenization sense. While this does not affect the comparative assessment performed in the present work, next-stage studies should perform systematic size-scaling analyses by progressively increasing the number of unit cells while preserving topology and relative density. Numerical homogenization techniques and periodic boundary conditions could then be used to determine representative volume elements and evaluate the convergence of effective properties such as stiffness, strength, Poisson's ratio, and energy absorption.

The present study therefore demonstrates the effectiveness of combining twinning-inspired architectures with topology optimization under controlled uniaxial compression, but several scientific and technological challenges must be addressed before the proposed design framework can be translated into practical engineering applications. At the same time, these challenges define some of the most promising future research directions.

A first challenge concerns scalability. Although the stress-delocalization and load-redistribution mechanisms identified in this work are expected to remain valid across different length scales, the relative contribution of buckling, yielding, and manufacturing-induced imperfections may change significantly as the architecture is miniaturized or enlarged. Future studies should therefore establish scaling relationships through multi-scale simulations and experimental validation across different structural dimensions.

A second challenge is associated with manufacturing implementation. While PolyJet technology offers excellent geometric fidelity and was therefore ideal for validating the proposed concepts, its cost and production throughput may limit large-scale deployment. Future developments should investigate alternative additive-manufacturing routes and systematically assess the influence of manufacturing defects, dimensional tolerances, and process-induced variability on the mechanical response of the optimized architectures.

Another important aspect concerns fatigue resistance and multi-axial loading. The present study focuses on monotonic compression and therefore does not address long-term durability under cyclic loading or the response under combined compression, tension, bending, torsion, and shear. Future investigations should combine fatigue testing with fatigue-informed numerical modeling and extend the optimization framework toward multi-load-case design strategies representative of real engineering environments.

Additionally, other promising research directions concern the quantitative characterization of deformation localization. While the present study identifies the emergence of shear bands through DIC measurements and PEEQ distributions, a rigorous evaluation of parameters such as shear-band width, local strain gradients, accumulated plastic dissipation, and energy partitioning requires dedicated image-guided failure assessment methodologies. The extraction of such quantities is highly dependent on image resolution, strain-field filtering, threshold selection, and localization criteria, making direct comparison across architectures non-trivial. Future work will therefore focus on the development of robust image-based characterization procedures capable of quantitatively describing the evolution of shear bands and their relationship with damage accumulation and failure propagation in architected metamaterials.

It should be noted that the present study was intentionally restricted to a single relative density in order to isolate the effects of twinning and topology optimization from density-related influences. Consequently, density-dependent scaling laws and Gibson–Ashby coefficients could not be established. Future investigations should therefore consider multiple relative-density levels and alternative lattice families to determine scaling relationships for stiffness, strength, ductility, and energy absorption, enabling direct benchmarking of the proposed framework against established architected-material systems.

Finally, among the most promising future directions is the development of multi-material and damage-programmable metamaterials. By combining twinning-induced stress delocalization with topology optimization and spatially tailored material distributions, highly stressed regions could be reinforced with high-performance materials while less critical zones remain lightweight and compliant. Such architectures could enable controlled deformation pathways, localized energy dissipation, and predictable failure mechanisms. More broadly, coupling these strategies with advanced finite-element modeling, multi-objective optimization, and emerging multi-material additive-manufacturing technologies could enable architected materials specifically designed for application-dependent responses. This approach would pave the way toward resilient, adaptive, and damage-aware metamaterials for safety–critical applications such as aerospace structures, impact-protection systems, and next-generation biomedical implants.

4. Conclusions

This study demonstrates that integrating Nature-inspired twinning with topology optimization significantly enhances the mechanical performance of architected lattices. Experimental results show that the *twinned* lattice achieves ≈20% higher ductility relative to the *baseline* structure, while the *optimized* lattice exhibits an ≈97 % increase in ductility and ≈118 % increase in peak load, confirming the effectiveness of the combined design strategy. Finite-element simulations accurately capture stress pathways and shear-band formation, validating the model for comparative analyses. These findings highlight that sequential architectural modifications, twinning followed by optimization, enable controlled stress redistribution, delay failure, and maximize energy absorption. The results further indicate that twinning and topology optimization contribute through distinct but complementary mechanisms, with twinning governing deformation localization and topology optimization enhancing load-bearing efficiency. These outcomes provide a quantitative foundation for the design of high-performance architected materials and indicate clear potential for multi-material and damage-programmable metamaterials in applications requiring predictable deformation and enhanced structural resilience.

CRediT authorship contribution statement

F. Buccino: Writing – review & editing, Writing – original draft, Validation, Investigation, Funding acquisition, Conceptualization. **L. Matteucci:** Investigation, Data curation. **M. Mirzaali:** Resources, Investigation. **A. Zadpoor:** Resources, Investigation. **L.M. Vergani:** Writing – review & editing, Validation, Supervision, Methodology, Investigation, Funding acquisition, Conceptualization.

Declaration of competing interest

The authors declare that they have no known competing financial interests or personal relationships that could have appeared to influence the work reported in this paper.

Acknowledgements

The authors acknowledge Dr. Vahid Moosabeiki Dehabadi for assisting in the experimental tests.

F.B., M.M. A.Z. and L.M.V. acknowledge the financial support from the European Union Horizon Europe research and innovation programme under the Horizon Europe research and innovation programme EIC Pathfinder Challenges under grant agreement No 101161602 (PANTAREI).

F.B. acknowledges financial support from the Italian Ministry of University and Research (MUR) through the Fondo Italiano per la Scienza (FIS 3) programme, under project IDEM (CUP D53C25002420001).

Appendix A. Supplementary data

Supplementary data to this article can be found online at https://doi.org/10.1016/j.matdes.2026.116576.

Data availability

The data supporting this article have been included as part of the Supplementary Information.

References

[1] Z. Alomar, F. Concli, Compressive behavior assessment of a newly developed circular cell-based lattice structure, Mater. Des. 205 (2021) 109716, https://doi.org/10.1016/j.matdes.2021.109716.
[2] N. Kladovasilakis, K. Tsongas, D. Karalekas, D. Tzetzis, Architected Materials for Additive Manufacturing: a Comprehensive Review, Materials 15 (2022) 5919, https://doi.org/10.3390/ma15175919.
[3] W. Wu, S. Kim, A. Ramazani, Y. Tae Cho, Twin mechanical metamaterials inspired by nano-twin metals: Experimental investigations, Compos. Struct. 291 (2022) 115580, https://doi.org/10.1016/j.compstruct.2022.115580.
[4] A.A. Zadpoor, Mechanical meta-materials, Mater. Horiz. 3 (2016) 371–381, https://doi.org/10.1039/C6MH00065G.
[5] G. Burns, A.M. Glazer, the 14 Bravais Lattices, in: Space Groups for Solid State Scientists, Springer Berlin Heidelberg, 1990: pp. 34–54. https://doi.org/10.1016/b978-0-08-096412-6.50008-8.
[6] A.G. Jackson, Handbook of Crystallography, Springer, N. Y. (1991), https://doi.org/10.1007/978-1-4612-3052-6.
[7] A.A. Salem, S.R. Kalidindi, R.D. Doherty, Strain hardening of titanium: Role of deformation twinning, Acta Mater. 51 (2003) 4225–4237, https://doi.org/10.1016/S1359-6454(03)00239-8.
[8] Z. Jia, F. Liu, X. Jiang, L. Wang, Engineering lattice metamaterials for extreme property, programmability, and multifunctionality, J. Appl. Phys. 127 (2020), https://doi.org/10.1063/5.0004724.
[9] G. Martinoia, The helical leitmotiv in Nature: towards tailored torsion-resistant bio-inspired solutions, (2022).
[10] F. Buccino, G. Martinoia, L.M. Vergani, Torsion—resistant structures: a nature addressed solution, Materials 14 (2021) 5368, https://doi.org/10.3390/ma14185368.
[11] Z. Li, X. Li, Z. Wang, W. Zhai, Multifunctional sound-absorbing and mechanical metamaterials via a decoupled mechanism design approach, Mater. Horiz. 10 (2023) 75–87, https://doi.org/10.1039/D2MH00977C.
[12] Y. Wei, F. Pan, X. Lin, L. Zhang, J. Xiang, Y. Chen, On-demand Reprogrammable Mechanical Metamaterial Driven by Structure Performance Relations, Adv. Mater. 37 (2025), https://doi.org/10.1002/ADMA.202410865.
[13] M. Yu, X. Fang, D. Yu, Metamaterials with in situ tunable bending properties, Mater. Horiz. (2026), https://doi.org/10.1039/D5MH02063H.
[14] J. Shi, J. Luo, C. Liu, H. Chu, Y. Jing, C. Xu, X. Liu, J. Li, Y. Lai, From directional to omnidirectional: meta-devices for ultrabroadband sound absorption with near-causality-limit performance, Mater. Horiz. 12 (2025) 9262–9271, https://doi.org/10.1039/D5MH00404G.
[15] J. Wang, X. Zhang, Twinning effects on strength and plasticity of metallic materials, MRS Bull. 41 (2016) 274–281, https://doi.org/10.1557/mrs.2016.67.
[16] J. Liu, R. Niu, J. Gu, Y. Liu, S. Ni, J. Cariney, M. Song, Y.-W. Mai, T. Zhu, X. Liao, Effects of twinning configurations on the mechanical performance of small-scale FCC metallic materials, Acta Mater. 306 (2026) 121880, https://doi.org/10.1016/J.ACTAMAT.2025.121880.

[17] E. El-Danaf, S.R. Kalidindi, R.D. Doherty, Influence of grain size and stacking-fault energy on deformation twinning in fcc metals, Metall. Mater. Trans. A Phys. Metall. Mater. Sci. 30 (1999) 1223–1233, https://doi.org/10.1007/s11661-999-0272-9.
[18] M. Calcagnotto, Y. Adachi, D. Ponge, D. Raabe, Deformation and fracture mechanisms in fine- and ultrafine-grained ferrite/martensite dual-phase steels and the effect of aging, Acta Mater. 59 (2011) 658–670, https://doi.org/10.1016/j.actamat.2010.10.002.
[19] M. Maurizi, C. Gao, F. Berto, Inverse design of truss lattice materials with superior buckling resistance, npj Comput. Mater. 8 (2022), https://doi.org/10.1038/s41524-022-00938-w.
[20] M. Maurizi, B.W. Edwards, C. Gao, J.R. Greer, F. Berto, Fracture resistance of 3D nano-architected lattice materials, Extreme Mech. Lett. 56 (2022) 101883, https://doi.org/10.1016/j.eml.2022.101883.
[21] N.K. Katiyar, G. Goel, S. Hawi, S. Goel, Nature-inspired materials: Emerging trends and prospects, NPG Asia Mater. 13 (2021) 1–16, https://doi.org/10.1038/s41427-021-00322-y.
[22] S.M. Ahmadi, G. Campoli, S. Amin Yavari, B. Sajadi, R. Wauthle, J. Schrooten, H. Weinans, A.A. Zadpoor, Mechanical behavior of regular open-cell porous biomaterials made of diamond lattice unit cells, J. Mech. Behav. Biomed. Mater. 34 (2014) 106–115, https://doi.org/10.1016/j.jmbbm.2014.02.003.
[23] J. Kadkhodapour, H. Montazerian, A.C. Darabi, A.P. Anaraki, S.M. Ahmadi, A. A. Zadpoor, S. Schmauder, Failure mechanisms of additively manufactured porous biomaterials: Effects of porosity and type of unit cell, J. Mech. Behav. Biomed. Mater. 50 (2015) 180–191, https://doi.org/10.1016/j.jmbbm.2015.06.012.
[24] E. Chen, S. Luan, S. Gaitanaros, On the compressive strength of brittle lattice metamaterials, Int. J. Solids Struct. 257 (2022), https://doi.org/10.1016/j.ijsolstr.2022.111871.
[25] K. Liang, Z. Wei, X. Zhang, Machine learning based inverse design of variable stiffness mechanical metamaterials, Int. J. Mech. Sci. 312 (2026) 111265, https://doi.org/10.1016/J.IJMECSCI.2026.111265.
[26] M.S. Pham, C. Liu, I. Todd, J. Lertthanasarn, Damage-tolerant architected materials inspired by crystal microstructure, Nature 565 (2019) 305–311, https://doi.org/10.1038/s41586-018-0850-3.
[27] Z. Li, K.G. Pradeep, Y. Deng, D. Raabe, C.C. Tasan, Metastable high-entropy dual-phase alloys overcome the strength-ductility trade-off, Nature 534 (2016) 227–230, https://doi.org/10.1038/nature17981.
[28] Y. Zhang, J. Zhang, X. Zhao, Y. Li, S. Che, W. Yang, L. Han, Mechanical behaviors regulation of triply periodic minimal surface structures with crystal twinning, Addit. Manuf. 58 (2022) 103036, https://doi.org/10.1016/j.addma.2022.103036.
[29] Y. Liu, L. St-Pierre, N.A. Fleck, V.S. Deshpande, A. Srivastava, High fracture toughness micro-architectured materials, J. Mech. Phys. Solids 143 (2020) 104060, https://doi.org/10.1016/j.jmps.2020.104060.
[30] C. Pan, Y. Han, J. Lu, Design and optimization of lattice structures: a review, Applied Sciences (switzerland) 10 (2020) 1–36, https://doi.org/10.3390/APP10186374.
[31] S. Kechagias, R.N. Oosterbeek, M.J. Munford, S. Ghouse, J.R.T. Jeffers, Controlling the mechanical behaviour of stochastic lattice structures: the key role of nodal connectivity, Addit. Manuf. 54 (2022) 102730, https://doi.org/10.1016/j.addma.2022.102730.
[32] S.M. Ahmadi, S.A. Yavari, R. Wauthle, B. Pouran, J. Schrooten, H. Weinans, A. A. Zadpoor, Additively manufactured open-cell porous biomaterials made from six different space-filling unit cells: the mechanical and morphological properties, Materials 8 (2015) 1871–1896, https://doi.org/10.3390/ma8041871.
[33] F. Wang, M. Brøns, O. Sigmund, Non-Hierarchical Architected Materials with Extreme Stiffness and Strength, Adv. Funct. Mater. 33 (2023), https://doi.org/10.1002/adfm.202211561.
[34] X. Zheng, H. Lee, T.H. Weisgraber, M. Shusteff, J. DeOtte, E.B. Duoss, J.D. Kuntz, M.M. Biener, Q. Ge, J.A. Jackson, S.O. Kucheyev, N.X. Fang, C.M. Spadaccini, Ultralight, ultrastiff mechanical metamaterials, Science 344 (2014) (1979) 1373–1377, https://doi.org/10.1126/science.1252291.
[35] T. Gangwar, D. Schillinger, Microimaging-informed continuum micromechanics accurately predicts macroscopic stiffness and strength properties of hierarchical plant culm materials, Mech. Mater. 130 (2019) 39–57, https://doi.org/10.1016/j.mechmat.2019.01.009.
[36] F. Libonati, C. Colombo, L. Vergani, Design and characterization of a biomimetic composite inspired to human bone, Fatigue Fract. Eng. Mater. Struct. 37 (2014) 772–781, https://doi.org/10.1111/ffe.12172.
[37] J.H. Zhang, X.J. Wei, Y. Zhang, J.S. Liu, Z.K. Mi, Y.C. Qu, L. Hua, T. Ding, T. Cheng, J. Cai, Y.M. Xie, X. Ren, Chiral twisting metamaterials with bilayer helical rod, Int. J. Mech. Sci. 315 (2026) 111437, https://doi.org/10.1016/J.IJMECSCI.2026.111437.
[38] G. Zappa, L. Cocchi, S. Candidori, F. Buccino, L. Vergani, S. Graziosi, Twinning-inspired hexagonal close-packed metamaterials for enhanced energy absorption, Mater. Des. 244 (2024) 113098, https://doi.org/10.1016/j.matdes.2024.113098.
[39] F. Liang, B. Zhang, S. Wang, J. Nan, Y. Lin, Y. Li, W. Chen, H. Wan, Y. Zhu, X. Chen, Twinning-dominated scratch mechanism transitions in commercial pure Titanium from micro to macro scales, Acta Mater. 296 (2025) 121254, https://doi.org/10.1016/j.actamat.2025.121254.
[40] D. You, A.S.K. Mohammed, M. Nishida, H. Sehitoglu, Origin of twinning mode hierarchy in NiTi – a critical understanding, Acta Mater. 302 (2026) 121645, https://doi.org/10.1016/j.actamat.2025.121645.
[41] C. Paramatmuni, F.P.E. Dunne, Effect of stress-states on non-classical twinning in three-point bending of magnesium alloys, Int. J. Mech. Sci. 258 (2023) 108574, https://doi.org/10.1016/J.IJMECSCI.2023.108574.
[42] M. Ateeq, L.M. Vergani, F. Buccino, M. Ateeq, L.M. Vergani, F. Buccino, Integration of Multi-Scale Predictive Tools of Bone Fragility: A Structural and Material Property Perspective, Materials 2025, Vol. 18, 18 (2025). https://doi.org/10.3390/MA18194639.
[43] F. Buccino, F. Giuseppoli, T. Kochetkova, J. Schwiedrzik, L.M. Vergani, Advances in nanoscopic mechanobiological structure-property relationship in human bones for tailored fragility prevention, Mater. Today Commun. 40 (2024) 1–5, https://doi.org/10.1016/j.mtcomm.2024.110108.
[44] D. Taylor, Fracture mechanics: how does bone break? Nat. Mater. 2 (2003) 133–134, https://doi.org/10.1038/nmat843.
[45] Y. Zhang, C. He, Q. Yu, X. Li, X. Wang, Y. Zhang, J. Wang, C. Jiang, Y. Jia, X. C. Zhang, B. Sun, R.O. Ritchie, S.T. Tu, Nacre-like surface nanolaminates enhance fatigue resistance of pure titanium, Nat. Commun. 15 (2024) 6917, https://doi.org/10.1038/s41467-024-51423-5.
[46] R. Wang, H.S. Gupta, Deformation and fracture mechanisms of bone and nacre, Annu. Rev. Mater. Res. 41 (2011) 41–73, https://doi.org/10.1146/annurev-matsci-062910-095806.
[47] F. Buccino, I. Aiazzi, A. Casto, B. Liu, M.C. Sbarra, G. Ziarelli, L.M. Vergani, S. Bagherifard, Down to the bone: a novel bio-inspired design concept, Materials 14 (2021) 4226, https://doi.org/10.3390/ma14154226.
[48] F. Libonati, V. Cipriano, L. Vergani, M.J. Buehler, Computational Framework to Predict failure and Performance of Bone-inspired Materials, ACS Biomater Sci. Eng. 3 (2017) 3236–3243, https://doi.org/10.1021/acsbiomaterials.7b00606.
[49] F. Libonati, A.E. Vellwock, F. Ielmini, D. Abliz, G. Ziegmann, L. Vergani, Bone-inspired enhanced fracture toughness of de novo fiber reinforced composites, Sci. Rep. 9 (2019) 1–12, https://doi.org/10.1038/s41598-019-39030-7.
[50] C. Lendlein, N.Y.J. Tan, Twin-inspired design for strengthening and toughening of lightweight lattices in plastic deformation, MRS Commun. 15 (2025) 300–307, https://doi.org/10.1557/s43579-025-00712-1.
[51] H. Liu, D. Lin, L. Yang, S. Wu, Y. Ren, R. Xiong, S. Leng, H.S. Kim, C. Yan, Y. Shi, Enhanced mechanical responses and fatigue behaviors of triply periodic minimal surface lattice metamaterials by twin-oriented lattice design, Int. J. Fatigue 201 (2025) 109172, https://doi.org/10.1016/J.IJFATIGUE.2025.109172.
[52] N. Zhang, X. Ma, Y. Chang, X. Tian, A lattice structure with adjustable mechanical behavior constructed by rotating triangles translated out of plane and splicing each other, Int. J. Solids Struct. 292 (2024) 112740, https://doi.org/10.1016/J.IJSOLSTR.2024.112740.
[53] M.L.S. Hedvard, M.A. Dias, M.K. Budzik, Toughening mechanisms and damage propagation in Architected-Interfaces, Int. J. Solids Struct. 288 (2024) 112600, https://doi.org/10.1016/J.IJSOLSTR.2023.112600.
[54] W. Zhao, J. Zhu, L. Liu, J. Leng, Y. Liu, A bio-inspired 3D metamaterials with chirality and anti-chirality topology fabricated by 4D printing, Int. J. Smart Nano Mater. 14 (2023) 1–20, https://doi.org/10.1080/19475411.2022.2120110.
[55] Z. Gao, X. Zhang, Y. Wu, M.S. Pham, Y. Lu, C. Xia, H. Wang, H. Wang, Damage-programmable design of metamaterials achieving crack-resisting mechanisms seen in nature, Nat. Commun. 15 (2024) 1–12, https://doi.org/10.1038/s41467-024-51757-0.
[56] Y. Wang, Y. Lei, R. Cui, Y. Jin, D. Halim, G.J. Cheng, B. Deng, A genus-tuning design on minimal surfaces for open-cell mechanical metamaterials, Int. J. Mech. Sci. 313 (2026) 111304, https://doi.org/10.1016/J.IJMECSCI.2026.111304.
[57] S. Fang, W. Xiao, K. Chen, X. Song, Research on the Model for the Friction Coefficient of Resin-based Friction Material and its Experimental Verification, Materials 16 (2023), https://doi.org/10.3390/ma16134791.
[58] L. Zhang, S. Feih, S. Daynes, Y. Wang, M.Y. Wang, J. Wei, W.F. Lu, Buckling optimization of Kagome lattice cores with free-form trusses, Mater. Des. 145 (2018) 144–155, https://doi.org/10.1016/J.MATDES.2018.02.026.
[59] D. Li, R. Qin, J. Xu, J. Zhou, B. Chen, Topology optimization of thin-walled tubes filled with lattice structures, Int. J. Mech. Sci. 227 (2022) 107457, https://doi.org/10.1016/j.ijmecsci.2022.107457.
[60] X. Huang, Y.M. Xie, G. Lu, Topology optimization of energy-absorbing structures, Int. J. Crashworthiness 12 (2007) 663–675, https://doi.org/10.1080/13588260701497862.
[61] A. Senatore, M. Venza, S. Candidori, S. Graziosi, F. Buccino, Enhancing bending and compression resistance of additively manufactured bio-inspired architected structures, European Journal of Mechanics, A/solids 111 (2025) 105557, https://doi.org/10.1016/j.euromechsol.2024.105557.
[62] M. Donofrio, Topology Optimization and Advanced Manufacturing as a Means for the Design of Sustainable Building Components, Procedia Eng. 145 (2016) 638–645, https://doi.org/10.1016/j.proeng.2016.04.054.
[63] J.S. Weeks, Mechanical Response of Lattice Structures under High Strain-Rate and shock Loading, California Institute of Technology (2023).
[64] J.C. Najmon, J. Dehart, Z. Wood, A. Tovar, Cellular helmet Liner Design through Bio-inspired Structures and Topology Optimization of Compliant Mechanism Lattices, SAE Int. J. Transp. Saf. 6 (2018) 217–235, https://doi.org/10.4271/2018-01-1057.
[65] P.E. Gill, M.A. Saunders, E. Wong, On the performance of SQP methods for nonlinear optimization, in: Springer Proceedings in Mathematics and Statistics, Springer International Publishing, 2015, pp. 95–123, https://doi.org/10.1007/978-3-319-23699-5_5.
[66] R. Liu, W. Chen, J. Zhao, A Review on Factors Affecting the Mechanical Properties of Additively-Manufactured Lattice Structures, J. Mater. Eng. Perform. 33 (2024) 4685–4711, https://doi.org/10.1007/s11665-023-08423-1.
[67] X. Shi, W. Liao, T. Liu, C. Zhang, D. Li, W. Jiang, C. Wang, F. Ren, Design optimization of multimorphology surface-based lattice structures with density gradients, Int. J. Adv. Manuf. Technol. 117 (2021) 2013–2028, https://doi.org/10.1007/s00170-021-07175-3.
[68] D. McArthur, P.J. Tan, C.L.A. Leung, Tuning the mechanical behaviour of additively manufactured meta-materials with twinning and meta-harmonics,

Virtual Phys. Prototyp. 20 (2025), https://doi.org/10.1080/17452759.2025.2512977.
[69] D. McArthur, G. Maddison, J. Vijayakumar, P. Tafforeau, K. Christofidou, P.D. Lee, P.J. Tan, C.L.A. Leung, Triply-Twinned Metamaterials: Unraveling the Mechanics and failure Pathways through High-Resolution XCT, Adv. Mater. 38 (2026) e16173, https://doi.org/10.1002/ADMA.202516173.
[70] R.O. Ritchie, M.J. Buehler, P. Hansma, Plasticity and toughness in bone, Phys. Today 62 (2009) 41–47, https://doi.org/10.1063/1.3156332.
[71] N. Aldegaither, G. Sernicola, A. Mesgarnejad, A. Karma, D. Balint, J. Wang, E. Saiz, S.J. Shefelbine, A.E. Porter, F. Giuliani, Fracture toughness of bone at the microscale, Acta Biomater. 121 (2021) 475–483, https://doi.org/10.1016/j.actbio.2020.12.007.
[72] M. Zouaoui, C. Labergere, J. Gardan, A. Makke, N. Recho, P. Lafon, Finite element modeling and anisotropy implementation in 3D printed structures using an optimized method, 24th French Congress of Mechanics (2019) 1–10.
[73] A.I. Pais, J.L. Alves, J. Belinha, A bio-inspired remodelling algorithm combined with a natural neighbour meshless method to obtain optimized functionally graded materials, Eng. Anal. Bound. Elem. 135 (2022) 145–155, https://doi.org/10.1016/j.enganabound.2021.10.016.
[74] S. Daynes, TPMS-based metamaterials with tuneable elastic anisotropy and mechanical coupling, Mater. Des. 253 (2025) 113866, https://doi.org/10.1016/J.MATDES.2025.113866.
[75] A. Askari, M. Jamalzadeh, A review of structural diversity design and optimization for lattice metamaterials, AIP Adv. 14 (2024), https://doi.org/10.1063/5.0229080/3316406.
[76] A. Alomarah, H.K. Dalfi, C. Rodrigo, D. Ruan, Compressive performances of 3D-bio-inspired auxetic metamaterials: Design and experiments, Thin-Walled Struct. 220 (2026) 114355, https://doi.org/10.1016/J.TWS.2025.114355.
[77] A. Alomarah, Y. Yuan, D. Ruan, A bio-inspired auxetic metamaterial with two plateau regimes: Compressive properties and energy absorption, Thin-Walled Struct. 192 (2023) 111175, https://doi.org/10.1016/J.TWS.2023.111175.